Acta Cryst C STRUCTURAL CHEMISTRY

ISSN 2053-2296

Two metastable high hydrates of energetic material 3,3′,5,5′-tetranitro-4,4′-bipyrazole

Kostiantyn V. Domasevitch[a]* and Harald Krautscheid[b]

[a]Inorganic Chemistry Department, National Taras Shevchenko University of Kyiv, Volodymyrska Str. 64/13, 01601 Kyiv, Ukraine, and [b]Institute of Inorganic Chemistry, Leipzig University, Johannisallee 29, D-04103 Leipzig, Germany. *Correspondence e-mail: dk@univ.kiev.ua

Received 6 March 2024
Accepted 16 April 2024

Edited by I. Oswald, University of Strathclyde, United Kingdom

Keywords: molecular hydrate; hydrogen bonding; N-heterocyclic aromatic compound; nitro compounds; lone pair–π-hole interaction; crystal structure; Ostwald rule.

CCDC references: 2348676; 2348675

Supporting information: this article has supporting information at journals.iucr.org/c

Poly-stoichiometry of hydrated phases is relatively uncommon for organic materials and extended libraries of such species adopting different aqua-to-substrate ratios are still rare. The kinetically controlled higher hydrates could be particularly interesting for their structural relationships, which presumably may imprint some features of the substrate/substrate and aqua/substrate bonding in solutions, and provide insights into the nucleation stage. Two metastable high hydrates are prepared by crash crystallization. The crystal structures of 3,3′,5,5′-tetranitro-4,4′-bipyrazole tetrahydrate, $C_6H_2N_8O_8{\cdot}4H_2O$, (1), and 3,3′,5,5′-tetranitro-4,4′-bipyrazole pentahydrate, $C_6H_2N_8O_8{\cdot}5H_2O$, (2), are intrinsically related to the previously reported anhydrate and monohydrate, while displaying natural evolution of the patterns upon progressive watering. The accumulation of the water molecules causes their clustering, with the generation of one-dimensional tapes and two-dimensional layers in the genuine channel hydrates (1) and (2), respectively, *versus* the pocket hydrate structure of $C_6H_2N_8O_8{\cdot}H_2O$. The hydration primarily affects the pyrazole sites. It conditions the emergence of N—H···O and O—H···N hydrogen bonds, which is a destructive factor for pyrazole/pyrazole N—H···N hydrogen bonding. At the same time, extensive noncovalent interactions of the organic molecules, namely, lone pair–π-hole O···N interactions of the NO_2/NO_2 and NO_2/pyrazole types, are more competitive to the hydrogen bonding and the motifs of mutual organic/organic stacks remain intact with the increase in hydration. These trends agree with the results of Hirshfeld surface analysis. The contributions of the contacts involving H atoms are increased in line with the growing number of water molecules, while the fraction of O···N/N···O (NO_2) contacts is nearly invariant. One may postulate the significance of the lone pair–π-hole interactions to the aggregation of nitro species in solutions and their relevance for the sebsequent development of the solid-state patterns through nucleation.

1. Introduction

Crystallization in the form of hydrates is inherent to many types of organic materials. These compositions are particularly significant to pharmaceutical science since the hydrated forms of active species may be more suited for applications with respect to long-term stability, solubility and drug performance (Morris, 1999). The general interest in organic hydrates is reflected in the increasing research interest in the crystal chemistry of such materials (Sanii *et al.*, 2021). A recently reported data-driven and topological mapping approach allows the prediction of hydrate crystal structures from an anhydrous framework (Hong *et al.*, 2022). It is believed that up to one third of organic compounds can afford hydrates (Stahly, 2007), while a recent analysis identified as many as 23698 unique hydrate structures within 286752 entries matching the search criteria (Werner & Swift, 2020). The existence of hydrated and anhydrous structures for a given compound is also

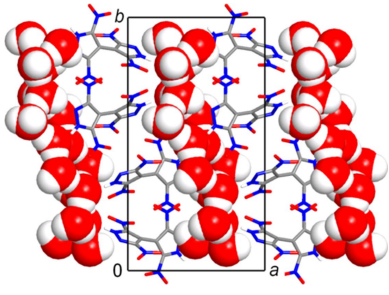

Table 1
Experimental details.

Experiments were carried out at 183 K with Cu $K\alpha$ radiation using a STOE STADIVARI diffractometer. Absorption was corrected for by multi-scan methods (*LANA*; Koziskova *et al.*, 2016).

	(1)	(2)
Crystal data		
Chemical formula	$C_6H_2N_8O_8{\cdot}4H_2O$	$C_6H_2N_8O_8{\cdot}5H_2O$
M_r	386.22	404.24
Crystal system, space group	Orthorhombic, *Pbca*	Monoclinic, $P2_1/c$
a, b, c (Å)	21.4196 (8), 6.1927 (2), 21.9265 (8)	11.2164 (5), 20.8114 (6), 6.6646 (3)
α, β, γ (°)	90, 90, 90	90, 90.435 (4), 90
V (Å^3)	2908.44 (18)	1555.67 (11)
Z	8	4
μ (mm^{-1})	1.53	1.51
Crystal size (mm)	0.10 × 0.07 × 0.05	0.09 × 0.07 × 0.03
Data collection		
T_{min}, T_{max}	0.771, 0.927	0.787, 0.963
No. of measured, independent and observed [$I > 2\sigma(I)$] reflections	20365, 3101, 2195	14058, 3321, 2619
R_{int}	0.038	0.041
$(\sin\theta/\lambda)_{max}$ (Å^{-1})	0.638	0.638
Refinement		
$R[F^2 > 2\sigma(F^2)]$, $wR(F^2)$, S	0.035, 0.092, 0.90	0.046, 0.128, 1.00
No. of reflections	3101	3321
No. of parameters	276	296
No. of restraints	32	53
H-atom treatment	All H-atom parameters refined	H atoms treated by a mixture of independent and constrained refinement
$\Delta\rho_{max}$, $\Delta\rho_{min}$ (e Å^{-3})	0.20, −0.23	0.42, −0.32

Computer programs: *X-AREA* (Stoe & Cie, 2016), *SHELXS97* (Sheldrick, 2008), *SHELXL2019* (Sheldrick, 2015), *DIAMOND* (Brandenburg, 1999) and *WinGX* (Farrugia, 2012).

remarkable. Only 1476 hydrates had a corresponding anhydrate in the database, although this number was possibly underestimated due to a bias of the Cambridge Structural Database (CSD; Groom *et al.*, 2016) toward structures that have only been crystallized once (Cruz-Cabeza *et al.*, 2015). Such an underestimation could be even more significant when considering the existence of hydrated and anhydrous structures as a special issue of a more general case of poly-stoichiometry of hydrates. Therefore, organic compositions with different substrate-to-aqua ratios are apparently uncommon, as revealed by the analysis of Basford (2021). Only seven compounds within a set of 6575 entries adopted at least three different hydrate stoichiometries. One may suppose that the number of such systems is still limited primarily at the expense of metastable and elusive higher hydrate forms, the existence of which can be foreseen with a degree of certainty for many cases.

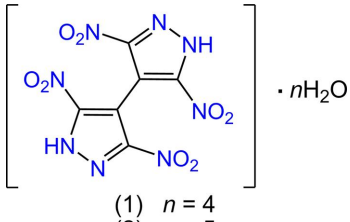

(1) $n = 4$
(2) $n = 5$

Scheme 1

Poly-stoichiometry of hydrates and the isolation of higher hydrates are particularly interesting in view of nucleation and crystal growth, since the crystallization of anhydrous or less hydrated forms inevitably succeeds significant desolvation of the dissolved species. Following the well-known Ostwald's rule of stages, one can intuitively assume initial crystallization of metastable highly hydrated phases. They may also be a primary outcome of crash crystallization. Such higher hydrates may inherit some features of the substrate–water interactions in solution, as a sufficient amount of the coordinated solvent remains an integral part of the crystal (Nangia & Desiraju, 1999). This situation is illustrated by the crystal structure of hexamethylenetetramine hexahydrate, bearing a close resemblance to the solution environment of the substrate (Burton *et al.*, 2009). Although crystallizations of hydrates often do not obey the rule of stages (Tian *et al.*, 2010), such a scenario may be more realistic for compounds that are most prone to forming hydrates. For example, 2,4-dihydroxybenzoic acid usually forms a hemihydrate, but fast cooling of hot solutions (crash crystallization) led to a very unstable monohydrate (Braun *et al.*, 2011).

The propensity of organic compounds for hydrate formation was associated with a (dis)balance of the available hydrogen-bond donor and acceptor sites (Desiraju, 1991), while a subsequent study suggested correlation rather with a total number of such functionalities within the molecule (Infantes *et al.*, 2007). With the aim of isolating high hydrates, we have explored the behaviour of 3,3′,5,5′-tetranitro-4,4′-bipyrazole (H_2Tnbpz), which is an excellent candidate for providing a set of valuable pre-requisites. First, this substrate perfectly fits the above criteria, in view of the exceptionally

rich hydrogen-bonding functionality accompanied by a striking mismatch between the numbers of available donors and acceptors, *i.e.* two N—H donors and ten O- and N-atom acceptors. Second, conformational flexibility of the bipyrazole molecule is largely beneficial for polymorphism and pseudo-polymorphism, which are well known for the 3,3′,5,5′-tetramethyl-4,4′-bipyrazole prototype (H_2Me_4bpz; Boldog *et al.*, 2003). An even more important functional feature is that the highly acidic N—H groups are very strong donors, while the NO_2 groups, as well as the weakly basic dinitropyrazole N atoms, are only poor acceptors of hydrogen bonding. In accordance with Etter's hydrogen-bonding rule (Etter, 1990), the need for the bonding of strong proton donors and acceptors here are to be implemented preferably in the case of the substrate–aqua pair. Therefore, unlike the N—H···N hydrogen-bonded patterns seen for the H_2Me_4bpz systems (Boldog *et al.*, 2001), rather N—H···OH_2 interactions may occur in the case of H_2Tnbpz. One can identify this substrate as being particularly prone either to hydrate formation or to hydrate poly-stoichiometry. Following these inputs, we succeeded in the crystallization of two metastable high hydrates and report their structures here. 3,3′,5,5′-Tetranitro-4,4′-bipyrazole and its ionic derivatives have attracted attention as perspective energetic materials, which combine sufficient performance and low sensitivity for safe applications (Gospodinov *et al.*, 2024).

2. Experimental

2.1. Synthesis and crystallization

3,3′,5,5′-Tetranitro-4,4′-bipyrazole was prepared by the nitration of 4,4′-bipyrazole in mixed acids (yield 92%) and was crystallized from hot water (45.0 g per 1 l) as the monohydrate (Domasevitch *et al.*, 2019).

To prepare the high hydrates, 0.0636 g (0.6 mmol) of solid Na_2CO_3 was added to a suspension of 0.3980 g (1.2 mmol) of $H_2Tnbpz{\cdot}H_2O$ in 7 ml of deionized water, and the mixture was stirred until gas evolution ceased. The mixture was then heated to 363–368 K to dissolve any solids, giving a clear light-yellow solution. Fast crystallization to a final temperature of 283 K (in ice) led to the formation of a voluminous deposit of very thin plates of $H_2Tnbpz{\cdot}5H_2O$, (2), filling the entire volume of the mixture. When the mixture was allowed to stand at room temperature for several hours, this initial product lost crystallinity and gradually disappeared. Instead, a cotton-like material crystallized, representing very thin needles of $H_2Tnbpz{\cdot}4H_2O$, (1). This new phase was stable when standing in the mother solution for 10–15 d, but eventually it also dissolved and compact blocks of the thermodynamically stable monohydrate were formed. Both (1) and (2) lost crystallinity in air within minutes. Single crystals were selected immediately after crystallization, but it was not possible to perform characterization of the materials by microanalysis.

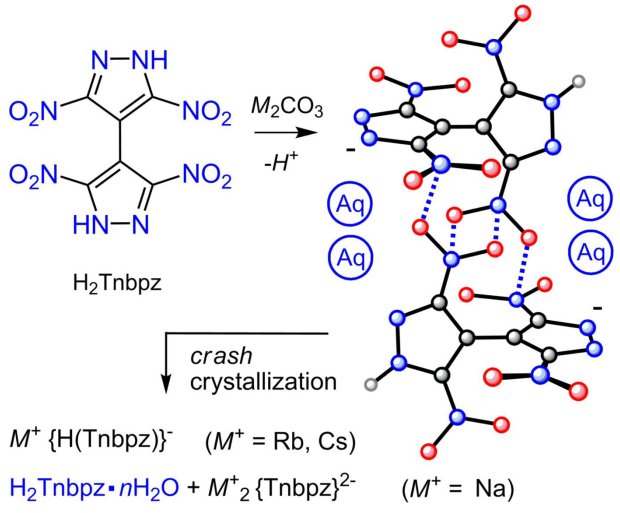

Figure 1
Crystallization of $H_2Tnbpz{\cdot}nH_2O$ as a result of prototropic dismutation of hydrogen bipyrazolates (M = Na). The postulated aggregation of the $H(Tnpbz)^-$ anions by extensive mutual NO_2/NO_2 interactions and hydration of the pyrazole sites are well reflected by the structures of the metastable high hydrates (1) and (2).

2.2. Refinement

Crystal data, data collection and structure refinement details are summarized in Table 1. All H atoms were located in difference maps and then refined with isotropic displacement parameters and with soft similarity restraints for the O—H bond lengths, which results in O—H = 0.87 (2)–0.88 (2) Å for (1) and 0.828 (17)–0.875 (17) Å for (2). For (1), the N—H bond lengths were restrained at 0.90 (3) Å. For (2), one of the water molecules is unequally disordered over two closely separated positions. The partial occupancy factors of 0.86/0.14 and the separation between the contributions were refined from an isotropic model and then fixed. The O atom of the minor component was left isotropic and the H atoms were constrained as riding, with O–H = 0.85 Å.

3. Results and discussion

The anhydrate H_2Tnbpz (CSD refcode PITGEH) crystallized with difficulty, using the Schlenk technique, from hot high-boiling aromatic solvents after azeotropic removal of any dissolved water (Domasevitch *et al.*, 2019). A strong trend for the hydration is best reflected by the formation of stable $H_2Tnbpz{\cdot}H_2O$ (refcode PITGIL), which dominated crystallization of the substrate from every examined common solvent under contact with ambient air. In spite of such invariant isolation of the monohydrate, further insights into this presumably rich hydrate system are possible when exploiting the special protolytic properties of H_2Tnbpz. Due to the appreciable acidity of 3,5-dinitropyrazole groups [pK_a = 3.14 for 3,5-dinitropyrazole; Janssen *et al.*, 1973], the substrate readily forms nitropyrazolate salts, such as $Li_2(Tnbpz)(H_2O)_4$ (Domasevitch *et al.*, 2023). Singly charged hydrogen bipyrazolate anions, $[H(Tnbpz)]^-$, are also known (Gospodinov *et al.*, 2020). Aqueous solutions of $M^I[H(Tnbpz)]$ may be pre-

Table 2
Hydrogen-bond geometry (Å, °) for (1).

D—H···*A*	*D*—H	H···*A*	*D*···*A*	*D*—H···*A*
N1—H1N···O1*W*	0.96 (2)	1.68 (2)	2.634 (2)	177 (3)
N5—H2N···O4*W*^{i}	0.97 (2)	1.76 (2)	2.723 (2)	172 (3)
O1*W*—H1···O3*W*	0.87 (2)	2.00 (2)	2.866 (2)	178 (3)
O1*W*—H2···O2*W*	0.87 (2)	1.97 (2)	2.771 (2)	153 (3)
O2*W*—H3···N6^{ii}	0.87 (2)	2.10 (2)	2.942 (2)	164 (3)
O2*W*—H4···O4*W*^{iii}	0.88 (2)	2.07 (2)	2.939 (2)	168 (3)
O3*W*—H5···O3^{iv}	0.86 (2)	2.31 (3)	3.116 (2)	156 (4)
O3*W*—H6···O2*W*^{iii}	0.88 (2)	1.90 (2)	2.766 (2)	170 (3)
O4*W*—H7···O3*W*	0.88 (2)	1.92 (2)	2.779 (2)	166 (3)
O4*W*—H8···O4^{v}	0.88 (2)	2.62 (4)	3.136 (2)	118 (3)
O4*W*—H8···O6^{iv}	0.88 (2)	2.39 (4)	3.051 (2)	132 (4)

Symmetry codes: (i) $-x, -y+1, -z+1$; (ii) $x+\frac{1}{2}, -y+\frac{1}{2}, -z+1$; (iii) $-x+\frac{1}{2}, y+\frac{1}{2}, z$; (iv) $x, -y+\frac{3}{2}, z+\frac{1}{2}$; (v) $x, -y+\frac{1}{2}, z+\frac{1}{2}$.

pared by neutralization with appropriate amounts of alkali metal carbonates, but the stability of such salts is rather different (Fig. 1). Hydrogen bipyrazolates were isolated with the largest Rb and Cs cations (Domasevitch & Ponomarova, 2021), but in the case of M^{I} = Li–K, they readily dismutated to afford soluble normal salts and the excess amount of the acid was deposited in the form of H_2Tnbpz·H_2O. However, we have found that the outcome of the crystallization depends on the cooling rate, and fast cooling of hot solutions allows the preparation of the metastable highly hydrated species (1) and (2).

The molecular structures of the title compounds are shown in Figs. 2 and 3. The main geometries of the organic frames agree well with the parameters for H_2Tnbpz and its monohydrate (Domasevitch *et al.*, 2019). In particular, clear differentiation of the angles at the ring N atoms suggests neutral pyrazole structures with localized and immobile H atoms [N—N(H)—C = 110.35 (15)–111.34 (14)° and N(H)—N—C = 103.74 (14)–105.11 (15)°]. Certain conjugation between the nitro groups and heterocycles is indicated by the nearly flat structure of the dinitropyrazole fragments, with corresponding NO_2/ring dihedral angles in a range 1.36 (9)–13.52 (11)° [mean 5.09 (14) and 6.97 (12)° for (1) and (2), respectively]. The dihedral angles between two pyrazole rings, however, are significant, being 66.95 (7)° for (1) and 60.38 (7)° for (2). For

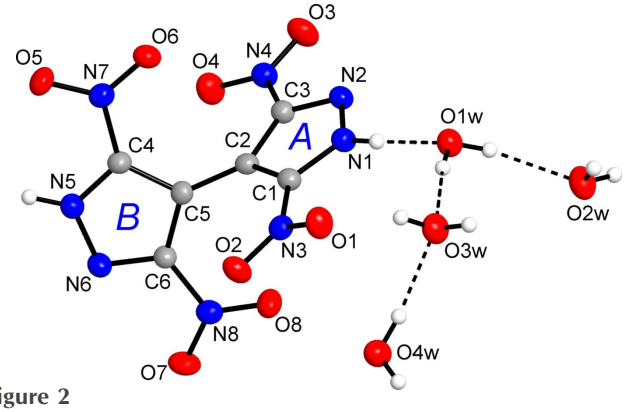

Figure 2
The molecular structure of H_2Tnbpz tetrahydrate, (1), showing the atom and ring labelling, and with displacement ellipsoids drawn at the 50% probability level. Dotted lines indicate hydrogen bonding.

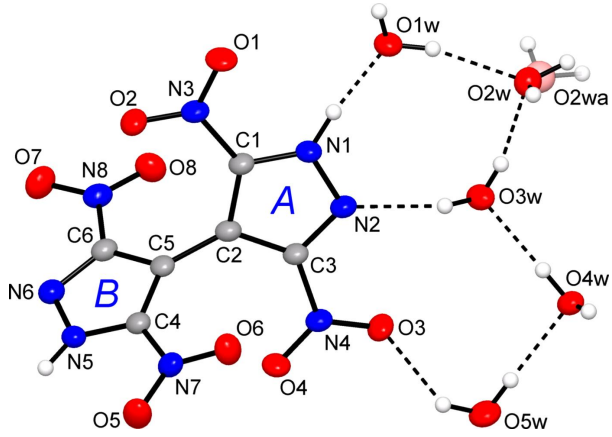

Figure 3
The molecular structure of H_2Tnbpz pentahydrate, (2), showing the atom and ring labelling, and with displacement ellipsoids drawn at the 50% probability level. One water molecule is unequally disordered (0.86:0.14) and the minor contribution (O2*WA*) is isotropic. Dotted lines indicate hydrogen bonding.

H_2Tnbpz·H_2O, this angle was even more appreciable [78.99 (6)°]. In spite of such a twisted conformation of the organic molecules, in each of the hydrates, the components afford relatively dense packing, as is indicated by packing indices of 73.6 for the monohydrate, 74.2 for (1) and 73.0 for (2), which are slightly higher than the value of 72.2 for the anhydrate structure. These values approach the upper limit of the 65–75% range expected for organic solids (Dunitz, 1995).

Progressive hydration results in a very illustrative evolution of crystal patterns (Fig. 4). H_2Tnbpz·H_2O was a genuine pocket hydrate incorporating isolated water molecules, whereas the two present metastable materials are channel hydrates showing extensive aqua–aqua hydrogen bonding. An increase in the molar fraction of water molecules does not lead to their uniform distribution in the lattice, but primarily causes clustering and the formation of extended hydrate networks. An immediate result of the clustering is the assembly of one-dimensional (1D) hydrate tapes in tetrahydrate (1), but with a higher number of water molecules in pentahydrate (2), the system develops an assembly of two-dimensional (2D) hydrate layers. In both structures, the mutual bonding of water molecules is directional and follows a standard geometry with typical O···O separations, which are 2.685 (2)–2.949 (3) Å for (1) (Table 2) and 2.766 (2)–2.939 (2) Å for (2) (Table 3). The longer O2*W*—H4···O5*W*^{i} hydrogen bond in (1) [O···O = 2.949 (3) Å and H···O = 2.33 (3) Å; symmetry code: (i) $-x, -y+1, -z+1$], however, exists as a shorter branch of a bifurcated interaction with aqua and nitro acceptors.

The infinite hydrate tapes in (1), running along the *b* direction in the crystal, consist of distorted seven-membered rings sharing three water molecules between adjacent units, which is a rare T7(3) hydrate topology according to Infantes & Motherwell (2002). The H_2Tnbpz molecules are integrated into the tape by double hydrogen bonding, but this scheme is relevant only for rings *B*, which are N—H···O hydrogen-bond donors and O—H···N hydrogen-bond acceptors (Fig. 5). The

Table 3
Hydrogen-bond geometry (Å, °) for (2).

D—H···A	D—H	H···A	D···A	D—H···A
N1—H1N···O1W	0.92 (3)	1.70 (3)	2.610 (2)	173 (3)
N5—H2N···O4W^{i}	0.87 (2)	1.85 (2)	2.723 (2)	179 (2)
O1W—H1···O2W	0.87 (2)	1.99 (2)	2.833 (2)	163 (2)
O1W—H2···O5W^{ii}	0.86 (2)	1.84 (2)	2.685 (2)	170 (3)
O2W—H3···N6^{iii}	0.88 (2)	2.21 (3)	3.000 (2)	151 (3)
O2W—H4···O5W^{iv}	0.83 (2)	2.33 (3)	2.949 (3)	131 (3)
O2W—H4···O1^{v}	0.83 (2)	2.57 (3)	3.241 (3)	139 (3)
O3W—H5···N2	0.85 (2)	2.07 (2)	2.885 (2)	160 (2)
O3W—H6···O2W	0.83 (2)	1.99 (2)	2.802 (2)	166 (2)
O4W—H7···O3W^{iv}	0.88 (2)	1.87 (2)	2.735 (2)	173 (2)
O4W—H8···O3W	0.85 (2)	1.91 (2)	2.749 (2)	176 (3)
O5W—H9···O4W	0.85 (2)	1.94 (2)	2.784 (2)	175 (3)
O5W—H10···O3	0.86 (2)	2.19 (3)	2.910 (2)	141 (3)
O5W—H10···O8^{iv}	0.86 (2)	2.67 (3)	3.065 (2)	109 (2)

Symmetry codes: (i) $x-1, -y+\frac{1}{2}, z+\frac{1}{2}$; (ii) $-x+1, y-\frac{1}{2}, -z+\frac{1}{2}$; (iii) $x+1, y, z-1$; (iv) $x, -y+\frac{1}{2}, z-\frac{1}{2}$; (v) $-x+1, -y, -z$.

former bond is particularly strong [N5···O4W^{i} = 2.723 (2) Å], whereas relative weakness of the latter interaction [O2W···N6^{ii} = 2.942 (2) Å; symmetry codes: (i) $-x, -y+1, -z+1$; (ii) $x+\frac{1}{2}, -y+\frac{1}{2}, -z+1$] reflects the low basicity of the dinitropyrazole N atom. The interactions of the *A* rings are more complicated and only strong N—H···OH_2 hydrogen bonds are retained [N1···O1W = 2.634 (2) Å]. The resulting dinitropyrazole/aqua ensemble is bound to the adjacent dinitropyrazole ring as a triple donor of lone pair–π-hole interactions (Fig. 5). In particular, the N2 atom is situated nearly above the ring centroid, with an N2···*Cg*(ring *A*)^{iii} distance of 3.2492 (16) Å, while nitro–nitro O3···N4^{iii} and aqua–nitro O1W···N3^{iii} separations are as short as 3.031 (2) and 3.029 (2) Å, respectively [symmetry code: (iii) $-x+\frac{1}{2}, y+\frac{1}{2}, z$.]

The hydrogen-bonded pattern of the H_2Tnbpz molecules in (2) is simpler due to a uniform function of both pyrazole rings. Similar to the *B* rings in the tetrahydrate, strong N—H···O hydrogen bonds to water molecules [N···O = 2.610 (2) and 2.723 (2) Å] are accompanied by weaker O—H···N interactions with aqua donors [N···O = 2.885 (2) and 3.000 (2) Å]. With such different donor and acceptor bonding, each pyrazole ring is installed at the hydrate layer (Fig. 6) and with two pairs of such bonds, the H_2Tnbpz molecules are embedded

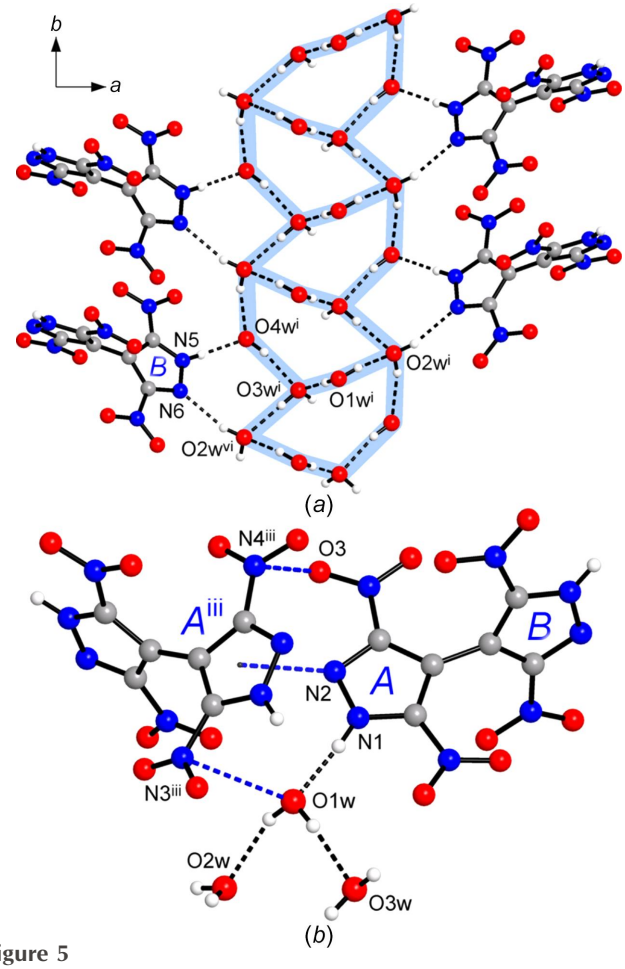

Figure 5
(*a*) Projection of the structure of (1) on the *ab* plane, showing the topology of the aqua tape (which is highlighted with a blue strip) and the accommodation of the H_2Tnbpz molecules through bonding of the *B* rings. (*b*) The bonding mode of the *A* rings with a set of lone pair–π-hole interactions involving also the O1W water molecule. [Symmetry codes: (i) $-x, -y+1, -z+1$; (iii) $-x+\frac{1}{2}, y+\frac{1}{2}, z$; (vi) $x-\frac{1}{2}, -y+\frac{1}{2}, -z+1$.]

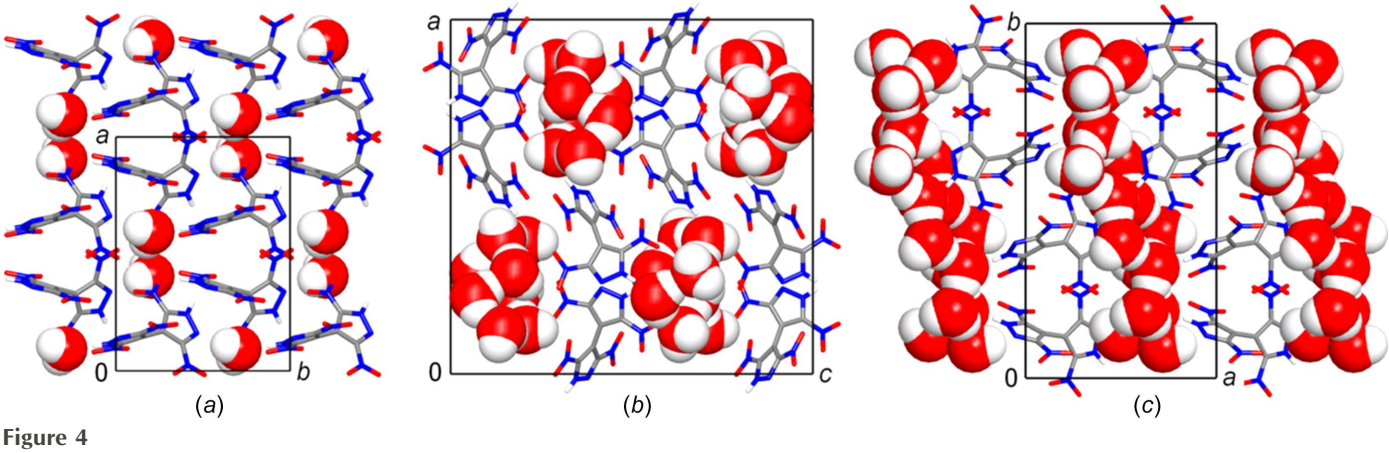

Figure 4
Evolution of the crystal patterns adopted by H_2Tnbpz·$n$$H_2O$ as a response to the increased number of water molecules. (*a*) The pocket hydrate PITGIL (n = 1), (*b*) the channel hydrate (1) (n = 4) embedding 1D aqua tapes and (*c*) the channel hydrate (2) (n = 5) with 2D aqua layers. For (*b*) and (*c*), the infinite aqua connectivities are orthogonal to the drawing plane.

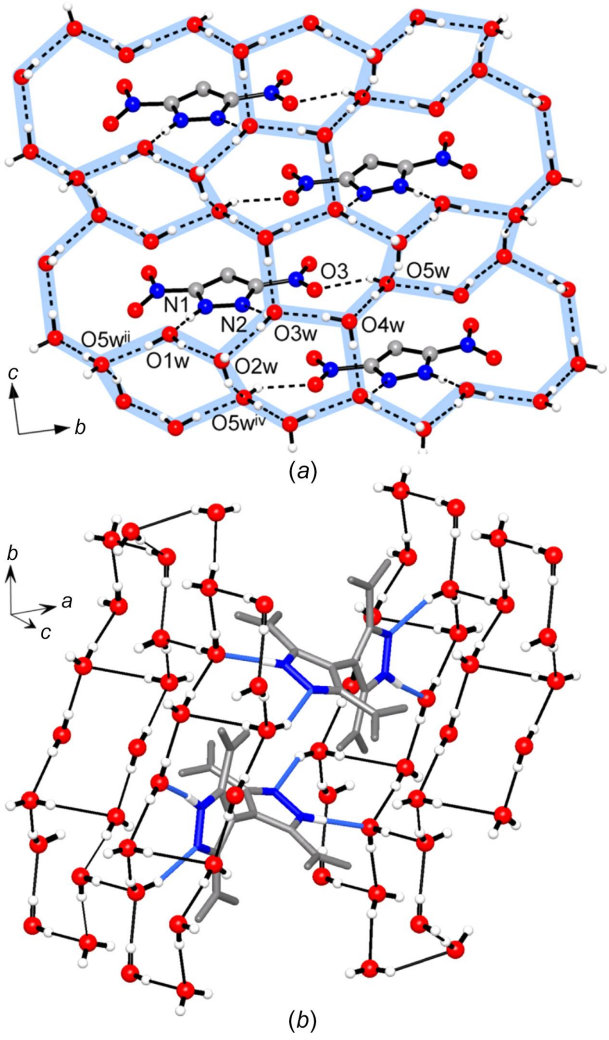

Figure 6
(*a*) Projection of the structure of (2) on the *bc* plane, showing the 2D aqua connectivity and how it integrates the organic molecules by multiple hydrogen bonding. (*b*) Two H_2Tnbpz molecules embedded between two successive hydrate layers, with the aqua shell wrapping the hydrophilic dinitropyrazole sites. [Symmetry codes: (ii) $-x+1, y-\frac{1}{2}, -z+\frac{1}{2}$; (iv) $x, -y+\frac{1}{2}, z-\frac{1}{2}$.]

between two hydrate layers separated by 11.2164 (5) Å, which is the *a* parameter of the unit cell.

Corrugation of the layer is conditioned by the need for the most effective interactions between the water molecules and the hydrophilic pyrazole sites. In fact, the water molecules tend to envelop dinitropyrazole groups, forming a certain sphere segment around them [Fig. 6(*b*)]. In this view, the array is reminiscent of the structures of clathrate hydrates incorporating the developed water frameworks. Such a structure could be assumed as a further possible step of the pattern evolution, with a higher water-to-substrate ratio. For example, the layered structure of 3-pyrroline trihydrate is similar to (2), but in the case of the pentahydrate, a genuine clathrate hydrate was observed (Rzepiński *et al.*, 2019).

However, unlike many relatively small molecules, such as 3-pyrroline, total encapsulation within the hydrate shell is hardly possible due to the very extensive and energetically

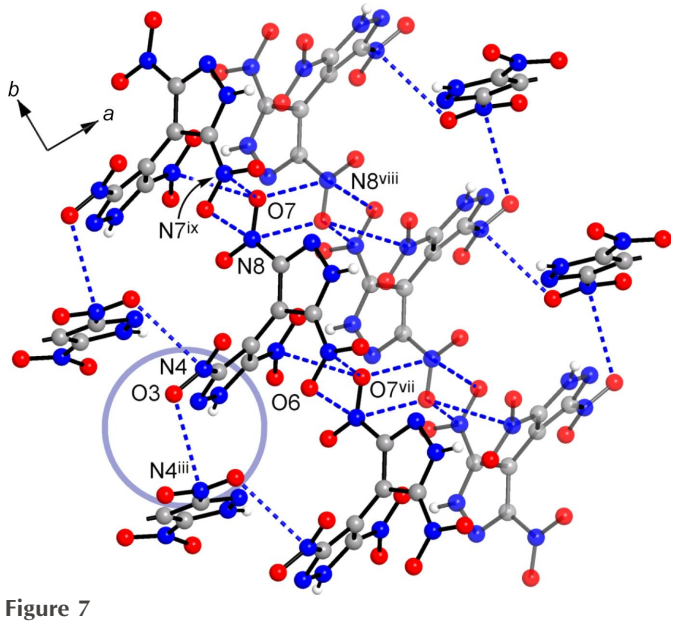

Figure 7
Lone pair–π-hole interactions of the NO_2 groups in the structure of (1), with the O7 atom acting as a triple donor of such bonds. The grey circle indicates a special kind of bonding involving *A* rings, which is further detailed in Fig. 5(*b*). [Symmetry codes: (iii) $-x+\frac{1}{2}, y+\frac{1}{2}, z$; (vii) $x, y+1, z$; (viii) $-x, -y, -z+1$; (ix) $x, y-1, z$.]

favourable interactions of the H_2Tnbpz molecules themselves. Mutual stacking of the NO_2 groups, as well as the stacking of NO_2 and pyrazole groups, which are kinds of peculiar lone pair–π-hole interactions (Bauzá *et al.*, 2015), are particularly prevalent and such bonding may be traced either for the anhydrate or any of the three hydrates. With a cut-off of 3.30 Å, as many as five short N···O contacts involving the nitro groups and also one $O_2N\cdots OH_2$ contact of this type, assemble the molecules into tapes along the *b* axis in (1) (Fig. 7). We note the local motif with four doubly stacked NO_2 groups and O7 atoms involved in three N···O contacts in the range 3.008 (2)–3.277 (2) Å (Table 4). In the case of (2) (Fig. 8), infinite double stacks along the *c* axis are generated by (N4/O3/O4)/(N4/O3/O4)^{vii} interactions, with N···O = 3.019 (2) Å [symmetry code: (vii) $x, -y+\frac{1}{2}, z+\frac{1}{2}$]. These separations are comparable to the short NO_2/NO_2 stacking seen in Li_2-(Tnbpz)$(H_2O)_4$ [N···O = 3.0349 (15)–3.0887 (15) Å; Domasevitch *et al.*, 2023], although they are slightly longer than similar parameters for H_2Tnbpz itself [2.911 (2) Å; Domasevitch *et al.*, 2019]. However, all these interactions are highly directional, as is indicated by the nearly orthogonal orientation of the N···O axes with respect to the planes of the acceptor NO_2 groups (Table 4). The NO_2/pyrazole stacking in every case is selective to the N(H) sites, with the N···O separations down to 3.063 (2) Å for (1).

Dense NO_2/NO_2 networks give rise also to less favourable close O···O contacts. For (1), they are only slightly below the sum of the van der Waals radii, *e.g.* O7···O7^{viii} = 2.970 (3) Å [symmetry code: (viii) $-x, -y, -z+1$], whereas (2) reveals an exceptionally short nonbonded contact O4···O6^{vii} of 2.5963 (18) Å [symmetry code: (vii) $x, -y+\frac{1}{2}, z+\frac{1}{2}$]. This may be compared with inter-polyhedral O···O contacts of

Table 4
Geometry of lone pair–π-hole interactions (Å, °) for (1) and (2).

Compound	O-atom donor	Group	O···N	O···plane	φ
O···N (nitro)					
(1)	O3	(C3/N4/O3/O4)^{iii}	3.031 (2)	2.8316 (16)	69.10 (3)
	O6	(C6/N8/O7/O8)^{vii}	3.002 (2)	2.8835 (18)	73.85 (3)
	O7	(C4/N7/O5/O6)^{ix}	3.008 (2)	2.8201 (19)	69.64 (4)
	O7	(C1/N3/O1/O2)^{ix}	3.277 (2)	3.098 (2)	70.98 (5)
	O7	(C6/N8/O7/O8)^{viii}	3.085 (2)	2.951 (2)	73.05 (5)
	O1*W*	(C1/N3/O1/O2)^{iii}	3.029 (2)	2.8845 (19)	72.23 (4)
(2)	O3	(C3/N4/O3/O4)^{iv}	3.034 (2)	2.9979 (16)	81.16 (2)
	O4	(C3/N4/O3/O4)^{vii}	3.019 (2)	2.9866 (16)	81.65 (2)
	O6	(C6/N8/O7/O8)^{viii}	3.217 (2)	2.911 (2)	64.81 (4)
	O7	(C1/N3/O1/O2)^{ix}	3.175 (2)	3.0653 (18)	74.89 (3)
	O1*W*	(C1/N3/O1/O2)^{vi}	3.132 (2)	2.9153 (19)	68.56 (4)
O···N(H) (ring)					
(1)	O2	(N5/N6/C4/C5/C6)^{i}	3.144 (2)	3.0726 (16)	77.77 (3)
	O5	(N5/N6/C4/C5/C6)^{xiii}	3.063 (2)	2.770 (3)	64.73 (5)
(2)	O1	(N5/N6/C4/C5/C6)^{iv}	3.087 (2)	2.738 (3)	62.49 (5)
	O5	(N5/N6/C4/C5/C6)^{x}	3.0857 (19)	2.781 (2)	64.32 (5)
	O8	(N1/N2/C1/C2/C3)^{ix}	3.190 (2)	3.1830 (19)	86.20 (4)

Notes: O···plane is a distance of the O-atom donor to the mean plane of the nitro (pyrazole) group and φ is the angle of the O···N axis to the plane of the nitro (pyrazole) group. [Symmetry codes for (1): (iii) $-x+\frac{1}{2}, y+\frac{1}{2}, z$; (vii) $x, y+1, z$; (viii) $-x, -y, -z+1$; (ix) $x, y-1, z$, (xiii) $-x, y+\frac{1}{2}, -z+\frac{1}{2}$. Symmetry codes for (2): (iv) $x, -y+\frac{1}{2}$, ***z*?1/2 [PLEASE CLARIFY]**; (vi) $-x+1, -y, -z+1$; (vii) $x, -y+\frac{1}{2}, z+\frac{1}{2}$; (viii) $x, y, z-1$; (ix) $x, y, z+1$; (x) $-x, -y, -z+1$.]

2.687 (2) Å in the much more robust covalent framework of $NiSO_4$ (Wildner, 1990). Such an arrangement is likely essential for the instability of the present hydrate.

One can note that the NO_2/NO_2 stacking tolerates well the progressively increased intensity of the substrate–aqua interactions in line with the increased number of the water molecules ($H_2Tnbpz{\cdot}nH_2O$; n = 0, 1, 4 or 5). This lone pair–π bonding is highly competitive to weak hydrogen bonds with nitro groups (Bauzá *et al.*, 2017) and therefore different kinds of such stacks remain intact even in the present high hydrates. In spite of the gradually increased number of identified O—H···O(NO_2) hydrogen bonds, which is two for the monohydrate, three for (1) and four for (2) (Table 5), these interactions represent only the weakest hydrogen bonds in the structures [O···O = 2.910 (2)–3.241 (3) Å] and remain in the shadow of the apparently stronger mutual interactions of the nitro groups. This is contrary to the mutual hydrogen bonding of H_2Tnbpz molecules. Thus, four N—H···O/O···H—N hydrogen bonds per molecule in H_2Tnbpz itself were completely eliminated even in the case of the monohydrate, whereas two N—H···N/N···H—N hydrogen bonds still retained in $H_2Tnbpz{\cdot}H_2O$, but disappear irrevocably upon further hydration, in favour of stronger N—H···OH_2 and O—H···N hydrogen bonds.

The supramolecular interactions in the H_2Tnbpz systems were further assessed by Hirshfeld surface analysis (Spackman & Byrom, 1997; McKinnon *et al.*, 2004; Hirshfeld, 1977) performed with *CrystalExplorer17* (Turner *et al.*, 2017). The 2D fingerprint plots for the anhydrate PITGEH [Fig. 9(*a*)] and individual H_2Tnbpz molecules in the monohydrate PITGIL [Fig. 9(*b*)] and the present tetra- [Fig. 9(*c*)] and pentahydrates [Fig. 9(*d*)] indicate the prevalence of the hydrogen-bond and O···N/N···O interactions, while general features for the partial contributions of the different contacts are very infor-

Table 5
Number of the identified interactions per single H_2Tnbpz molecule adopted for different hydrate environments in the structures of anhydrate PITGEH, monohydrate PITGIL and high hydrates (1) and (2).

Bond type	PITGEH	PITGIL	(1)	(2)
NH···N/N···HN	2	2	–	–
NH···O/O···HN	4	–	–	–
NH···O*W*	–	1	2	2
N···HO*W*	–	1	2	2
O···HO*W*	–	2	3	4
N···O/O···N (NO_2)	8	4	7	6
N···O/O···N (ring)	10	10	4	6
O_2N···O*W*	–	1	1	1
π···O*W*	–	–	–	1
O(N)···π/π···O(N)	2	2	4	–
N···NO_2/O_2N···N	2	–	–	–
O···O (NO_2)^{a}	4	4	6	3

Note: (*a*) the number of O···O contacts below 3.05 Å adopted by nitro groups.

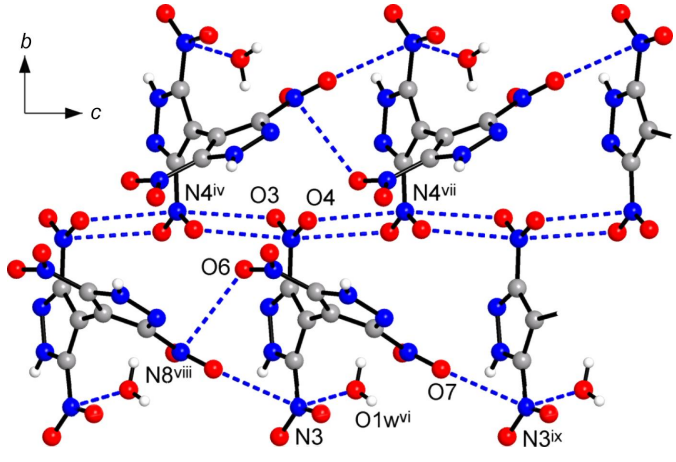

Figure 8
Lone pair–π-hole interactions of the NO_2 groups in the structure of (2), arranging the molecules into 1D stacks along the *c* direction. [Symmetry codes: (iv) $x, -y+\frac{1}{2}, z-\frac{1}{2}$; (vi) $-x+1, -y, -z+1$; (vii) $x, -y+\frac{1}{2}, z+\frac{1}{2}$; (viii) $x, y, z-1$; (ix) $x, y, z+1$.]

Table 6
Contributions of different kinds of the contacts (%) to the Hirshfeld surfaces of individual organic molecules in anhydrate PITGEH, monohydrate PITGIL and high hydrates (1) and (2).

For the two-dimensional plots for the principal contact, see Fig. 9.

Contacts	PITGEH	PITGIL	(1)	(2)
All···O,N	80.7	69.3	56.7	54.5
All···H	14.1	26.7	38.5	40.8
O···H/H···O	20.3	27.0	37.9	35.3
N···H/H···N	5.2	8.7	5.0	8.8
C···H/H···C	0.0	0.3	0.4	1.2
N···O/O···N	27.8	21.9	21.2	19.3
C···O/O···C	11.0	8.1	8.5	10.3
C···N/N···C	0.0	0.3	2.3	0.1
O···O	32.9	29.7	17.9	21.1
N···N	2.7	3.1	3.6	0.5
H···H	0.0	0.8	3.2	3.4

mative for the entire series (Table 6). The exceedingly large fraction of O···O contacts for H_2Tnbpz (32.9%) indicates essential contraction upon hydration, down to 29.7% for the monohydrate, 17.9% for (1) and 21.1% for (2). However, in the latter two cases, the packing generated shorter O···O contacts. This is particularly relevant for (2) and is reflected by a short spike pointing to the lower left, at $d_i + d_e$ = 2.6 Å [Fig. 6(*d*)]. The possible reasons for the ease of hydration of H_2Tnbpz, as well as for the instability of the present high hydrates, may be at least in part associated with the unfavourable O···O contacts between the nitro groups. A similar trend for decreased contributions of O···N/N···O contacts occurs primarily at the expense of less favourable NO_2/pyrazole interactions, since the fractions of entirely O···N/N···O (nitro) contacts themselves are almost insensitive to hydration (7.8–8.9%). The nature of the latter contacts is identical across the series and they are identified in the plots by symmetrical (about the diagonal where $d_i = d_e$) pairs of features. Therefore, both donor and acceptor sites of such bonds, namely, the O and N atoms of the nitro groups, appear within the individual H_2Tnbpz molecules. A slight shortening of these features reflects a certain weakening of the O···N bonds, which are 2.90 Å for H_2Tnbpz, 3.00 Å for (1) and 3.05 Å for (2). A decrease in the contribution of the O···O and O···N/N···O (pyrazole) contacts coincides with a rapid growth of contributions from the contacts with H atoms, which are only 14.1% for H_2Tnbpz and 26.7% for H_2Tnbpz·H_2O, but are 38.5% for (1) and even 40.8% for (2). Similar to $Li_2(Tnbpz)(H_2O)_4$ (Domasevitch *et al.*, 2023), it may be postulated that the water hydrogen-bond donors have only a minor influence on the lone pair–π-hole interactions of the nitro groups, but rather they help to avoid less favourable nitro-O···O contacts. Unlike the NO_2···NO_2 bonds, O···H/H···O bonds for the hydrates are visualized by asymmetric fingerprint plots, clearly suggesting the prevalence of the interactions with water molecules. The upper spikes are most sharp and their lengths indicate particularly short separations of H···O = 1.65 Å, corresponding to the strongest N—H···O*W* hydrogen bonds. Lower spikes indicate OH_2···O (nitro) bonds and they are perceptibly shorter (2.10–2.20 Å) and more diffuse. That the direct N—H···N hydrogen bonding between the pyrazole rings is irrelevant to the high hydrates coincides with the evolution of the upper spikes in the N···H/H···N plots. A very

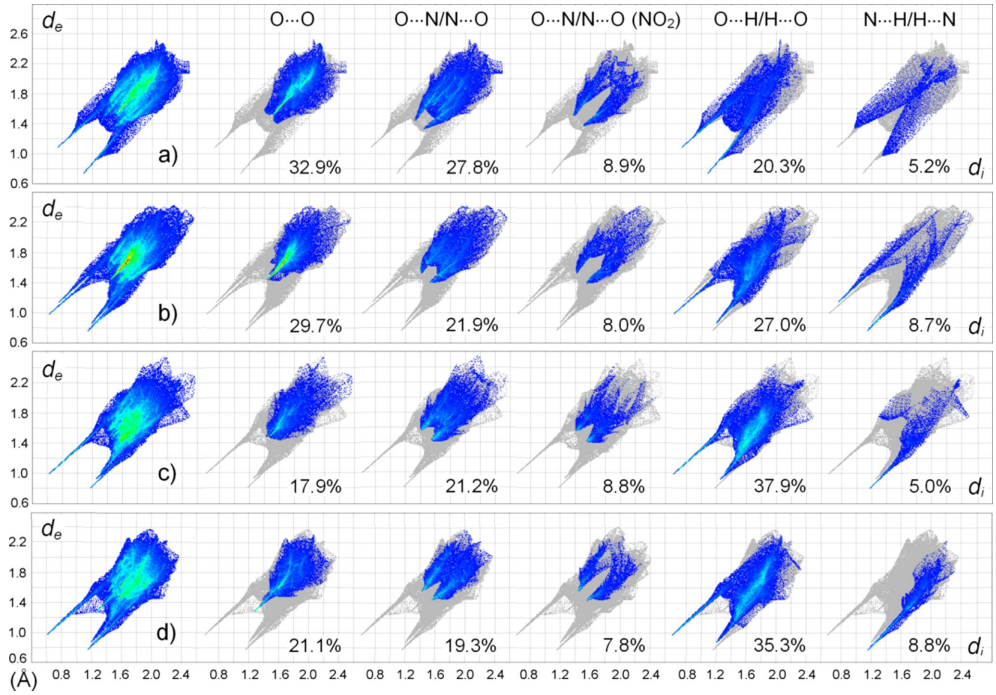

Figure 9
2D fingerprint plots for the individual H_2Tnbpz molecules, reflecting the subtle structural changes seen upon progressive hydration: (*a*) anhydrate PITGEH; (*b*) H_2Tnbpz·H_2O PITGIL; (*c*) H_2Tnbpz·$4H_2O$, (1); (*d*) H_2Tnbpz·$5H_2O$, (2), and delineated into the principal contributions of O···O, O···N/N···O, O···H/H···O and N···H/H···N contacts. For details on the other contributors to the surface areas, see Table 6.

Table 7
Calculated interaction energies (kJ mol^{-1}).

Interaction energies were calculated employing the CE-B3LYP/6-31G(d,p) functional/basis set combination. The scale factors used to determine E_{tot}: k_{ele} = 1.057, k_{pol} = 0.740, k_{dis} = 0.871 and k_{rep} = 0.618 (Mackenzie *et al.*, 2017).

Path	Type[a]	R (Å)	E_{ele}	E_{pol}	E_{dis}	E_{rep}	E_{tot}
(1)							
Org···Org^{ix}	*A*	6.19	−16.8	−3.2	−29.2	18.9	−33.9
Org···Org^{i}	*B*	6.29	−16.8	−3.1	−27.0	16.8	−33.3
Org···Org^{viii}	*C*	8.30	−2.9	−1.2	−14.1	8.6	−10.9
Org···Org^{x}	*D*	6.86	1.3	−4.1	−28.1	19.2	−14.3
Org···Org^{xi}	*E*	8.71	−7.4	−1.6	−8.8	4.2	−14.1
Org···(O1*W*)	NH···OH$_2$	5.54	−82.2	−20.1	−7.9	85.0	−56.1
Org···(O4*W*)^{i}	NH···OH$_2$	5.59	−62.8	−16.1	−6.9	56.8	−49.3
Org···(O2*W*)^{vi}	OH···N	5.90	−28.2	−4.7	−5.9	33.4	−17.8
Org···(O4*W*)^{xii}	OH···O	5.69	−12.0	−1.6	−5.9	11.1	−12.1
Org···(O3w)^{xii}	OH···O	5.09	0.4	−0.8	−4.1	3.0	−1.8
Org···(O1*W*)^{x}	H$_2$O···NO$_2$	4.50	−19.1	−4.1	−10.3	10.7	−25.5
(2)							
Org···Org^{iv}	*A*	6.66	−17.1	−2.7	−23.2	14.3	−31.5
Org···Org^{x}	*B*	6.10	−18.8	−3.4	−25.6	12.5	−37.0
Org···Org^{viii}	*C*	6.33	−14.7	−2.9	−29.6	22.3	−29.8
Org···Org^{xi}	*D*	8.35	−2.8	−1.3	−12.0	5.1	−11.2
Org···(O1*W*)	NH···OH$_2$	5.56	−83.7	−20.6	−6.7	87.3	−55.7
Org···(O4*W*)^{i}	NH···OH$_2$	5.61	−68.5	−17.5	−8.1	64.1	−52.9
Org···(O3w)	OH···N	5.72	−22.3	−5.0	−7.2	41.8	−7.8
Org···(O2*W*)^{xii}	OH···N	5.88	−11.9	−4.3	−6.5	24.1	−6.6
Org···(O4*W*)^{xiii}	OH···O	7.10	1.1	−0.4	−2.3	1.6	−0.1
Org···(O5*W*)	OH···O	6.77	−14.9	−2.1	−3.5	16.7	−10.0
Org···(O2*W*)^{v}	OH···O	6.21	−4.6	−0.8	−3.6	3.7	−6.3
Org···(O1*W*)^{vi}	H$_2$O···NO$_2$	4.43	−19.2	−3.6	−11.7	10.8	−26.4
Org···(O5*W*)^{vii}	H$_2$O···π	4.29	−4.2	−1.3	−7.2	3.2	−9.6

Notes: (*a*) For details of the interaction modes in (1), see Fig. 10, and for details of the interaction modes in (2), see Fig. 11; R is the distance between the centroids of the interacting molecules. Symmetry codes for (1): (i) $-x, -y+1, -z+1$; (vi) $x-\frac{1}{2}, -y+\frac{1}{2}, -z+1$; (viii) $-x, -y, -z+1$; (ix) $x, y-1, z$; (x) $-x+\frac{1}{2}, y-\frac{1}{2}, z$; (xi) $-x, y-\frac{1}{2}, -z+\frac{1}{2}$; (xii) $x, -y+\frac{3}{2}, z-\frac{1}{2}$. Symmetry codes for (2): (i) $x-1, -y+\frac{1}{2}, z+\frac{1}{2}$; (iv) $x, -y+\frac{1}{2}, z-\frac{1}{2}$; (v) $-x+1, -y, -z$; (vi) $-x+1, -y, -z+1$; (vii) $x, -y+\frac{1}{2}, z+\frac{1}{2}$; (viii) $x, y, z-1$; (x) $-x, -y, -z+1$; (xi) $-x, -y, -z+2$; (xii) $x-1, y, z+1$; (xiii) $x-1, y, z$.

diffuse collection of points at large $d_i + d_e$ seen for (1) completely disappears in the plot for the pentahydrate, leaving only a single lower sharp spike, which corresponds to OH$_2$···N bonds with H···N = 2.00 Å.

The intermolecular interaction energies were calculated using the CE B3LYP/6 31G(d,p) energy model in *CrystalExplorer17* (Turner *et al.*, 2017), where a set of symmetry-unique intermolecular paths were considered for the organic–organic and organic–aqua interactions for (1) and (2) (Table 7). From the plethora of intermolecular interactions, the highest energies (−49.3 to −56.1 kJ mol^{-1}) correspond to strong N—H···O hydrogen bonds established by highly acidic pyrazole N—H donors and the primary contributor to the total energy is the electrostatic component (up to −83.7 kJ mol^{-1}). These data are consistent with the energetics of azole–aqua interactions, which is E_{tot} = −23.9 kJ mol^{-1} for relatively weak donor pyrazole itself, but −41.4 kJ mol^{-1} for the pair sustained by acidic pentazole and water (Chopra *et al.*,

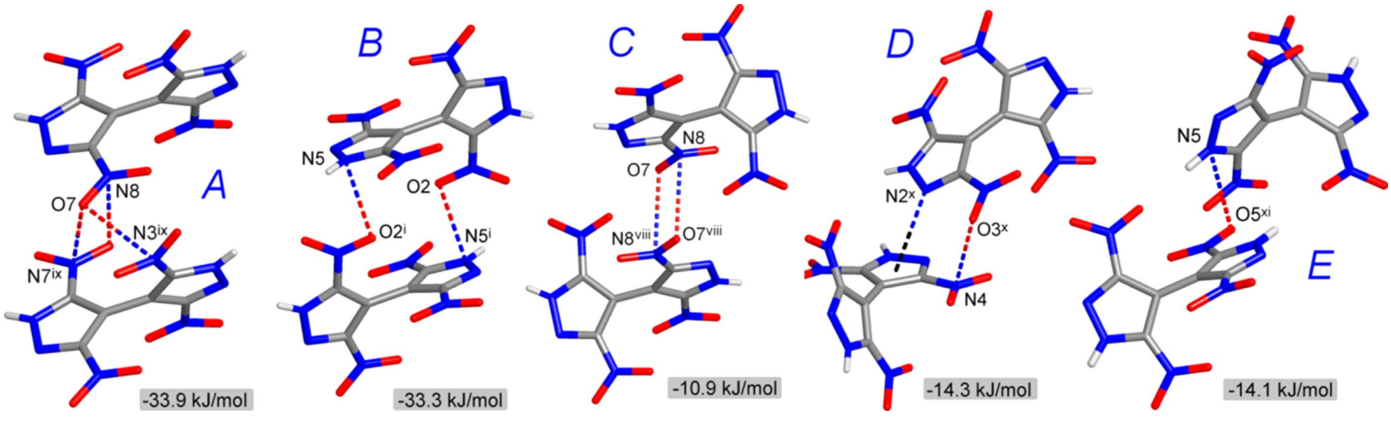

Figure 10
The five principal pathways (Types *A*–*E*) of the intermolecular bonding represented by different kinds of lone pair–π-hole interactions in the structure of (1). [Symmetry codes: (i) $-x, -y+1, -z+1$; (viii) $-x, -y, -z+1$; (ix) $x, y-1, z$; (x) $-x+\frac{1}{2}, y-\frac{1}{2}, z$; (xi) $-x, y-\frac{1}{2}, -z+\frac{1}{2}$.]

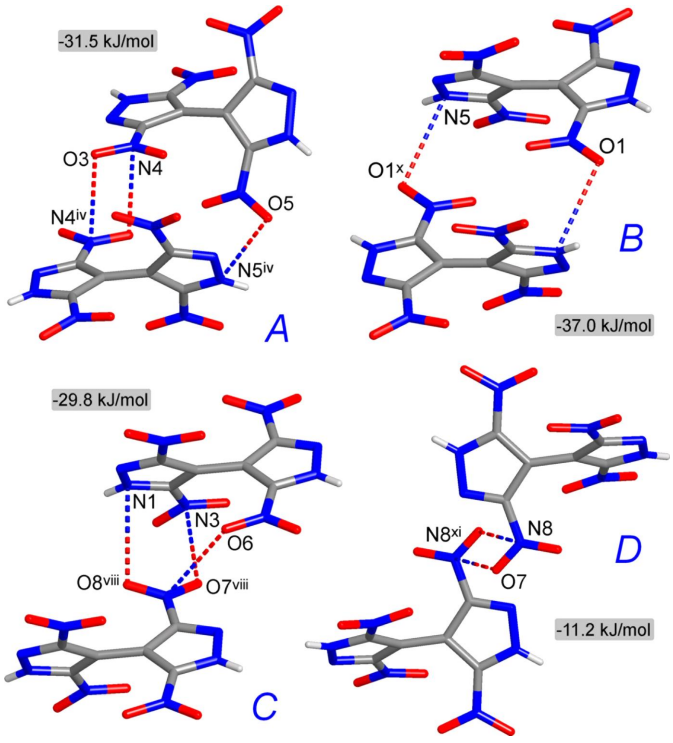

Figure 11
The NO_2/NO_2 and NO_2/pyrazole N···O interactions in the structure of (2). The double interactions of Type *D* are more distal [N···O = 3.432 (2) Å] and weaker. [Symmetry codes: (iv) $x, -y+\frac{1}{2}, z-\frac{1}{2}$; (viii) $x, y, z-1$; (x) $-x, -y, -z+1$; (xi) $-x, -y, -z+2$.]

2018). In the case of hydrogen bonding to weakly basic pyrazole N-atom acceptors, E_{tot} does not exceed −17.8 kJ mol^{-1}. However, such interactions are superior to the O—H···O hydrogen bonds with the nitro O-atom acceptors (Table 6). Beyond the particular N—H···O hydrogen bonds, the strongest organic–aqua interactions are lone pair–π-hole bonds with nitro N-atom acceptors, with E_{tot} approaching −26.4 kJ mol^{-1} in response to a higher contribution of the dispersion components. These values agree with the range of −8.5 to −33.6 kJ mol^{-1} reported for different nitro derivatives (Daszkiewicz, 2013).

It is not surprising that the E_{dis} contributors are essentially larger (up to −29.6 kJ mol^{-1}) for the different kinds of organic–organic stacks sustained by multiple lone pair–π-hole bonds. As a result, in every case, the total interaction energies are large and negative. This provides a realistic model for mutual stackings of H_2Tnbpz, which could be rival for interactions with the solvent by weaker O—H···O hydrogen bonds or single H_2O···NO_2 bonds. This emphasis is important when involving a certain pre-nucleation effect for the crystallization of the present high hydrates (1) and (2). In the case of (1), the highest energies are associated with the formation of pairs according to Type *A* (E_{tot} = −33.9 kJ mol^{-1}), with double O···N (nitro) bonding, and Type *B* (E_{tot} = −33.3 kJ $^{-1}$), with two inversion-related O···N (pyrazole) interactions (Fig. 10). Three different pairs (Types *A*–*C*; Fig. 11) occur for (2), with very comparable interaction energies up to −37.0 kJ mol^{-1} (Table 6). The energetics of the individual O···N (nitro) and O···N (pyrazole) interactions are very similar, as is suggested by the values calculated for Types *C* and *E* in (1), and Type *D* in (2) (E_{tot} are about −11 to −14 kJ mol^{-1}). The latter values slightly exceed the energies of most O—H···O hydrogen bonds with nitro acceptors. Therefore, the extensive organic–aqua interactions in (1) and (2) concern predominantly the outer hydrophylic pyrazole N/NH regions, whereas two kinds of lone pair–π-hole bonds with nitro groups provide the main motifs for the packing of shape-complementary H_2Tnbpz molecules. Also, the accumulation of additional organic–aqua interactions at the expense of the more favourable organic–organic bonding may be involved as a structure-destabilizing factor when comparing tetrahydrate (1) and very unstable pentahydrate (2).

In brief, the present systems provide an attractive paradigm for the crystallization of organic hydrates. The sequence of appearance of the various forms, moving from the exclusively unstable and elusive pentahydrate to the more stable tetrahydrate and finally to the stable monohydrate, is entirely consistent with Ostwald's rule of stages. The library of metastable high hydrates developed in the present study is important for the understanding of nucleation and crystal growth. In terms of Steed & Steed (2015), the metastable phases may be viewed as '*fossil relics of the fastest growing crystal nuclei*' and therefore they possibly reflect some preferable stacking configurations of the molecules and modes of their bonding with the solvent. Since the twisted molecules of 3,3′,5,5′-tetranitro-4,4′-bipyrazole, as well as the corresponding anionic species, perfectly fit one another like puzzle pieces and are prone to the generation of dense stacks, the postulated effects of pre-nucleation could be particularly significant in the present case. Therefore, this system may offer new insights not only into the area of organic hydrates, but also to the related problems of polymorphism and pseudo-polymorphism.

Funding information

Funding for this research was provided by: Ministry of Education and Science of Ukraine (grant No. 22BF037-11).

References

Basford, P. A. (2021). *Structural Relationships between Hydrates and Anhydrous Crystals: Towards Building an Understanding of Hydration in the Solid State*. PhD thesis, University of Manchester, England.
Bauzá, A., Mooibroek, T. J. & Frontera, A. (2015). *Chem. Commun.* **51**, 1491–1493.
Bauzá, A., Sharko, A. V., Senchyk, G. A., Rusanov, E. B., Frontera, A. & Domasevitch, K. V. (2017). *CrystEngComm*, **19**, 1933–1937.
Boldog, I., Rusanov, E. B., Chernega, A. N., Sieler, J. & Domasevitch, K. V. (2001). *Angew. Chem. Int. Ed.* **40**, 3435–3438.
Boldog, I., Rusanov, E. B., Sieler, J., Blaurock, S. & Domasevitch, K. V. (2003). *Chem. Commun.* pp. 740–741.
Brandenburg, K. (1999). *DIAMOND*. Release 2.1e. Crystal Impact GbR, Bonn, Germany.

Braun, D. E., Karamertzanis, P. G., Arlin, J.-B., Florence, A. J., Kahlenberg, V., Tocher, D. A., Griesser, U. J. & Price, S. L. (2011). *Cryst. Growth Des.* **11**, 210–220.
Burton, R. C., Ferrari, E. S., Davey, R. J., Finney, J. L. & Bowron, D. T. (2009). *J. Phys. Chem. B*, **113**, 5967–5977.
Chopra, N., Kaur, D. & Chopra, G. (2018). *ACS Omega*, **3**, 12688–12702.
Cruz-Cabeza, A. J., Reutzel-Edens, S. M. & Bernstein, J. (2015). *Chem. Soc. Rev.* **44**, 8619–8635.
Daszkiewicz, M. (2013). *CrystEngComm*, **15**, 10427–10430.
Desiraju, G. R. (1991). *J. Chem. Soc. Chem. Commun.* pp. 426–428.
Domasevitch, K. V., Gospodinov, I., Krautscheid, H., Klapötke, T. M. & Stierstorfer, J. (2019). *New J. Chem.* **43**, 1305–1312.
Domasevitch, K. V. & Ponomarova, V. V. (2021). *Acta Cryst.* E**77**, 1109–1115.
Domasevitch, K. V., Senchyk, G. A. & Krautscheid, H. (2023). *Acta Cryst.* E**79**, 657–663.
Dunitz, J. D. (1995). *X-ray Analysis and the Structure of Organic Solids*, 2nd corrected reprint, pp. 106–111. Basel: Verlag Helvetica Chimica Acta.
Etter, M. C. (1990). *Acc. Chem. Res.* **23**, 120–126.
Farrugia, L. J. (2012). *J. Appl. Cryst.* **45**, 849–854.
Gospodinov, I., Domasevitch, K. V., Unger, C. C., Benz, M., Stierstorfer, J. & Klapötke, T. M. (2024). *FirePhysChem* **4**, 1–9.
Gospodinov, I., Domasevitch, K. V., Unger, C. C., Klapötke, T. M. & Stierstorfer, J. (2020). *Cryst. Growth Des.* **20**, 755–764.
Groom, C. R., Bruno, I. J., Lightfoot, M. P. & Ward, S. C. (2016). *Acta Cryst.* B**72**, 171–179.
Hirshfeld, F. L. (1977). *Theor. Chim. Acta*, **44**, 129–138.
Hong, R. S., Mattei, A., Sheikh, A. Y. & Tuckerman, M. E. (2022). *Proc. Natl Acad. Sci. USA*, **119**, e2204414119.
Infantes, L., Fábián, L. & Motherwell, W. D. S. (2007). *CrystEngComm*, **9**, 65–71.
Infantes, L. & Motherwell, S. (2002). *CrystEngComm*, **4**, 454–461.
Janssen, J. W. A. M., Kruse, C. C., Koeners, H. J. & Habraken, C. (1973). *J. Heterocycl. Chem.* **10**, 1055–1058.
Koziskova, J., Hahn, F., Richter, J. & Kožíšek, J. (2016). *Acta Chim. Slov.* **9**, 136–140.
Mackenzie, C. F., Spackman, P. R., Jayatilaka, D. & Spackman, M. A. (2017). *IUCrJ*, **4**, 575–587.
McKinnon, J. J., Spackman, M. A. & Mitchell, A. S. (2004). *Acta Cryst.* B**60**, 627–668.
Morris, K. R. (1999). *Structural Aspects of Hydrates and Solvates*, in *Polymorphism in Pharmaceutical Solids*, ch. 4, edited by H. G Brittain. New York: Marcel Dekker.
Nangia, A. & Desiraju, G. R. (1999). *Chem. Commun.* pp. 605–606.
Rzepiński, P., Nowosielska, B., Cyrański, M. K., Boese, R. & Dobrzycki, L. (2019). *Cryst. Growth Des.* **19**, 4721–4730.
Sanii, R., Patyk-Kaźmierczak, E., Hua, C., Darwish, S., Pham, T., Forrest, K. A., Space, B. & Zaworotko, M. J. (2021). *Cryst. Growth Des.* **21**, 4927–4939.
Sheldrick, G. M. (2008). *Acta Cryst.* A**64**, 112–122.
Sheldrick, G. M. (2015). *Acta Cryst.* C**71**, 3–8.
Spackman, M. A. & Byrom, P. G. A. (1997). *Chem. Phys. Lett.* **267**, 215–220.
Stahly, G. P. (2007). *Cryst. Growth Des.* **7**, 1007–1026.
Steed, K. M. & Steed, J. W. (2015). *Chem. Rev.* **115**, 2895–2933.
Stoe & Cie (2016). *X-AREA*. Stoe & Cie GmbH, Darmstadt, Germany.
Tian, F., Qu, H., Zimmermann, A., Munk, T., Jørgensen, A. C. & Rantanen, J. (2010). *J. Pharm. Pharmacol.* **62**, 1534–1546.
Turner, M. J., McKinnon, J. J., Wolff, S. K., Grimwood, D. J., Spackman, P. R., Jayatilaka, D. & Spackman, M. A. (2017). *CrystalExplorer17*. University of Western Australia. http://crystalexplorer.scb.uwa.edu.au/.
Werner, J. E. & Swift, J. A. (2020). *CrystEngComm*, **22**, 7290–7297.
Wildner, M. (1990). *Z. Kristallogr.* **191**, 223–229.

supporting information

Acta Cryst. (2024). C**80**, 166-176 [https://doi.org/10.1107/S2053229624003346]

Two metastable high hydrates of energetic material 3,3′,5,5′-tetranitro-4,4′-bipyrazole

Kostiantyn V. Domasevitch and Harald Krautscheid

Computing details

3,3′,5,5′-Tetranitro-4,4′-bipyrazole tetrahydrate (1)

Crystal data

$C_6H_2N_8O_8·4H_2O$
M_r = 386.22
Orthorhombic, *Pbca*
a = 21.4196 (8) Å
b = 6.1927 (2) Å
c = 21.9265 (8) Å
V = 2908.44 (18) Å^3
Z = 8
F(000) = 1584
D_x = 1.764 Mg m^{-3}
Cu *Kα* radiation, *λ* = 1.54186 Å
Cell parameters from 14295 reflections
θ = 4.0–79.7°
μ = 1.53 mm^{-1}
T = 183 K
Needle, colorless
0.10 × 0.07 × 0.05 mm

Data collection

STOE STADIVARI diffractometer
Radiation source: GeniX 3D HF Cu
Graded multilayer mirror monochromator
Detector resolution: 5.81 pixels mm^{-1}
rotation method, *ω* scans
Absorption correction: multi-scan (LANA; Koziskova *et al.*, 2016)
T_{min} = 0.771, T_{max} = 0.927
20365 measured reflections
3101 independent reflections
2195 reflections with $I > 2\sigma(I)$
R_{int} = 0.038
θ_{max} = 79.8°, θ_{min} = 4.0°
h = −26→27
k = −7→2
l = −27→25

Refinement

Refinement on F^2
Least-squares matrix: full
$R[F^2 > 2\sigma(F^2)]$ = 0.035
$wR(F^2)$ = 0.092
S = 0.90
3101 reflections
276 parameters
32 restraints
Primary atom site location: structure-invariant direct methods
Secondary atom site location: difference Fourier map
Hydrogen site location: difference Fourier map
All H-atom parameters refined
$w = 1/[\sigma^2(F_o^2) + (0.0519P)^2]$ where $P = (F_o^2 + 2F_c^2)/3$
$(\Delta/\sigma)_{max} < 0.001$
$\Delta\rho_{max}$ = 0.20 e Å^{-3}
$\Delta\rho_{min}$ = −0.23 e Å^{-3}
Extinction correction: SHELXL2019 (Sheldrick, 2015), $Fc^* = kFc[1+0.001xFc^2\lambda^3/\sin(2\theta)]^{-1/4}$
Extinction coefficient: 0.00205 (15)

Special details

Geometry. All esds (except the esd in the dihedral angle between two l.s. planes) are estimated using the full covariance matrix. The cell esds are taken into account individually in the estimation of esds in distances, angles and torsion angles; correlations between esds in cell parameters are only used when they are defined by crystal symmetry. An approximate (isotropic) treatment of cell esds is used for estimating esds involving l.s. planes.

Fractional atomic coordinates and isotropic or equivalent isotropic displacement parameters (Å²)

	x	*y*	*z*	U_{iso}*/U_{eq}
O1	0.14098 (7)	0.6584 (2)	0.57023 (6)	0.0348 (3)
O2	0.06762 (7)	0.4647 (2)	0.52816 (6)	0.0344 (3)
O3	0.25768 (7)	0.5011 (3)	0.29894 (7)	0.0392 (3)
O4	0.16120 (7)	0.4025 (3)	0.28851 (6)	0.0382 (3)
O5	−0.00180 (7)	0.7610 (3)	0.28928 (7)	0.0383 (3)
O6	0.09120 (7)	0.8045 (2)	0.32791 (6)	0.0336 (3)
O7	0.02799 (7)	−0.1219 (2)	0.44849 (6)	0.0360 (3)
O8	0.11324 (7)	0.0525 (2)	0.47155 (7)	0.0390 (3)
N1	0.21495 (8)	0.6041 (3)	0.47257 (7)	0.0268 (3)
N2	0.24037 (7)	0.5836 (3)	0.41701 (7)	0.0266 (3)
N3	0.11831 (8)	0.5552 (3)	0.52746 (7)	0.0266 (3)
N4	0.20511 (8)	0.4678 (3)	0.31930 (7)	0.0285 (3)
N5	−0.01516 (7)	0.3807 (3)	0.34525 (7)	0.0270 (3)
N6	−0.01111 (7)	0.1998 (2)	0.37827 (7)	0.0267 (3)
N7	0.04235 (8)	0.7030 (3)	0.32128 (7)	0.0283 (3)
N8	0.06291 (8)	0.0349 (3)	0.44517 (7)	0.0280 (3)
C1	0.15489 (8)	0.5422 (3)	0.47268 (8)	0.0243 (3)
C2	0.13753 (8)	0.4775 (3)	0.41480 (7)	0.0234 (3)
C3	0.19343 (8)	0.5102 (3)	0.38276 (7)	0.0243 (3)
C4	0.03595 (8)	0.5028 (3)	0.35335 (7)	0.0240 (3)
C5	0.07673 (8)	0.4020 (3)	0.39341 (7)	0.0234 (3)
C6	0.04372 (8)	0.2129 (3)	0.40688 (7)	0.0235 (3)
O1W	0.28405 (7)	0.7280 (2)	0.56554 (6)	0.0330 (3)
O2W	0.37886 (7)	0.5771 (3)	0.64017 (7)	0.0385 (3)
O3W	0.21480 (8)	0.7967 (3)	0.67571 (7)	0.0364 (3)
O4W	0.12499 (8)	0.4908 (3)	0.70570 (7)	0.0361 (3)
H1N	0.2402 (13)	0.644 (5)	0.5067 (10)	0.060 (9)*
H2N	−0.0520 (12)	0.431 (5)	0.3242 (13)	0.071 (10)*
H1	0.2626 (13)	0.751 (5)	0.5985 (10)	0.065 (10)*
H2	0.3174 (11)	0.661 (5)	0.5777 (13)	0.055 (9)*
H3	0.4142 (12)	0.517 (5)	0.6312 (15)	0.074 (11)*
H4	0.3835 (17)	0.697 (5)	0.6616 (15)	0.097 (13)*
H5	0.2375 (17)	0.851 (7)	0.7040 (14)	0.102 (14)*
H6	0.1853 (12)	0.892 (4)	0.6691 (13)	0.067 (10)*
H7	0.1577 (13)	0.570 (5)	0.6966 (16)	0.084 (12)*
H8	0.127 (2)	0.474 (7)	0.7456 (11)	0.130 (17)*

Atomic displacement parameters (Å²)

	U^{11}	U^{22}	U^{33}	U^{12}	U^{13}	U^{23}
O1	0.0352 (8)	0.0409 (9)	0.0284 (6)	0.0001 (6)	−0.0029 (5)	−0.0098 (5)
O2	0.0297 (8)	0.0396 (9)	0.0340 (7)	−0.0074 (6)	0.0051 (6)	−0.0027 (5)
O3	0.0309 (8)	0.0486 (10)	0.0383 (7)	−0.0059 (6)	0.0113 (6)	−0.0026 (6)
O4	0.0352 (9)	0.0482 (10)	0.0312 (7)	−0.0031 (6)	−0.0007 (6)	−0.0073 (5)
O5	0.0353 (8)	0.0393 (9)	0.0402 (8)	0.0038 (6)	−0.0093 (6)	0.0113 (6)
O6	0.0324 (8)	0.0314 (8)	0.0370 (7)	−0.0056 (5)	0.0016 (6)	0.0063 (5)
O7	0.0411 (9)	0.0247 (8)	0.0421 (7)	−0.0071 (6)	0.0053 (6)	0.0024 (5)
O8	0.0345 (8)	0.0344 (9)	0.0481 (8)	0.0002 (6)	−0.0106 (6)	0.0082 (6)
N1	0.0266 (8)	0.0261 (8)	0.0278 (7)	−0.0022 (6)	−0.0003 (6)	−0.0002 (5)
N2	0.0240 (8)	0.0267 (9)	0.0292 (7)	−0.0024 (6)	0.0008 (6)	0.0019 (5)
N3	0.0283 (8)	0.0256 (9)	0.0259 (7)	0.0016 (6)	−0.0011 (6)	0.0000 (5)
N4	0.0272 (8)	0.0292 (9)	0.0289 (7)	0.0003 (6)	0.0034 (6)	−0.0003 (5)
N5	0.0253 (8)	0.0265 (9)	0.0291 (7)	0.0000 (6)	−0.0001 (6)	−0.0001 (5)
N6	0.0251 (8)	0.0228 (8)	0.0321 (7)	−0.0006 (5)	−0.0007 (6)	−0.0003 (5)
N7	0.0290 (8)	0.0289 (9)	0.0270 (7)	0.0016 (6)	0.0016 (6)	0.0023 (5)
N8	0.0296 (8)	0.0246 (9)	0.0299 (7)	−0.0004 (6)	0.0026 (6)	0.0001 (5)
C1	0.0238 (9)	0.0229 (9)	0.0263 (8)	−0.0003 (6)	0.0016 (6)	0.0010 (6)
C2	0.0251 (9)	0.0203 (9)	0.0248 (7)	−0.0007 (6)	0.0011 (6)	0.0017 (5)
C3	0.0238 (9)	0.0237 (9)	0.0254 (8)	−0.0004 (6)	0.0010 (6)	−0.0001 (6)
C4	0.0257 (9)	0.0224 (10)	0.0238 (7)	−0.0005 (6)	0.0007 (6)	0.0008 (5)
C5	0.0227 (9)	0.0237 (9)	0.0239 (7)	0.0014 (6)	0.0003 (6)	−0.0003 (5)
C6	0.0234 (8)	0.0212 (9)	0.0261 (8)	0.0000 (6)	−0.0003 (6)	0.0003 (5)
O1W	0.0296 (8)	0.0383 (9)	0.0312 (7)	−0.0018 (6)	−0.0023 (5)	−0.0008 (5)
O2W	0.0308 (8)	0.0362 (9)	0.0484 (8)	0.0016 (6)	−0.0038 (6)	−0.0076 (6)
O3W	0.0344 (8)	0.0396 (9)	0.0353 (7)	−0.0019 (6)	−0.0040 (6)	−0.0034 (5)
O4W	0.0351 (8)	0.0388 (9)	0.0344 (7)	−0.0054 (6)	−0.0034 (6)	0.0024 (6)

Geometric parameters (Å, º)

O1—N3	1.2343 (19)	N6—C6	1.334 (2)
O2—N3	1.222 (2)	N7—C4	1.432 (2)
O3—N4	1.229 (2)	N8—C6	1.445 (2)
O4—N4	1.226 (2)	C1—C2	1.382 (2)
O5—N7	1.231 (2)	C2—C3	1.403 (2)
O6—N7	1.229 (2)	C2—C5	1.461 (2)
O7—N8	1.228 (2)	C4—C5	1.387 (2)
O8—N8	1.228 (2)	C5—C6	1.399 (2)
N1—N2	1.340 (2)	O1W—H1	0.87 (2)
N1—C1	1.342 (2)	O1W—H2	0.87 (2)
N1—H1N	0.96 (2)	O2W—H3	0.87 (2)
N2—C3	1.335 (2)	O2W—H4	0.88 (2)
N3—C1	1.436 (2)	O3W—H5	0.86 (2)
N4—C3	1.438 (2)	O3W—H6	0.88 (2)
N5—N6	1.337 (2)	O4W—H7	0.88 (2)
N5—C4	1.342 (2)	O4W—H8	0.88 (2)

N5—H2N	0.97 (2)		
N2—N1—C1	111.34 (14)	N1—C1—N3	120.54 (15)
N2—N1—H1N	120.4 (17)	C2—C1—N3	129.62 (16)
C1—N1—H1N	127.9 (17)	C1—C2—C3	100.85 (15)
C3—N2—N1	103.74 (14)	C1—C2—C5	128.86 (16)
O2—N3—O1	125.27 (16)	C3—C2—C5	130.27 (15)
O2—N3—C1	118.00 (15)	N2—C3—C2	114.24 (15)
O1—N3—C1	116.74 (15)	N2—C3—N4	118.40 (16)
O4—N4—O3	123.93 (16)	C2—C3—N4	127.34 (16)
O4—N4—C3	117.35 (16)	N5—C4—C5	110.10 (16)
O3—N4—C3	118.71 (16)	N5—C4—N7	120.07 (16)
N6—N5—C4	110.35 (15)	C5—C4—N7	129.82 (17)
N6—N5—H2N	125.7 (19)	C4—C5—C6	101.07 (15)
C4—N5—H2N	123 (2)	C4—C5—C2	128.37 (16)
C6—N6—N5	105.11 (15)	C6—C5—C2	130.56 (16)
O6—N7—O5	124.88 (17)	N6—C6—C5	113.37 (15)
O6—N7—C4	117.78 (16)	N6—C6—N8	118.48 (16)
O5—N7—C4	117.33 (16)	C5—C6—N8	128.11 (16)
O7—N8—O8	125.24 (17)	H1—O1W—H2	105 (3)
O7—N8—C6	117.68 (16)	H3—O2W—H4	112 (3)
O8—N8—C6	117.09 (16)	H5—O3W—H6	105 (4)
N1—C1—C2	109.82 (15)	H7—O4W—H8	105 (3)
C1—N1—N2—C3	1.0 (2)	N6—N5—C4—N7	178.71 (14)
C4—N5—N6—C6	−0.10 (19)	O6—N7—C4—N5	−176.65 (16)
N2—N1—C1—C2	−0.5 (2)	O5—N7—C4—N5	3.7 (2)
N2—N1—C1—N3	−178.74 (15)	O6—N7—C4—C5	1.7 (3)
O2—N3—C1—N1	−168.07 (16)	O5—N7—C4—C5	−177.98 (18)
O1—N3—C1—N1	12.1 (2)	N5—C4—C5—C6	−0.02 (19)
O2—N3—C1—C2	14.1 (3)	N7—C4—C5—C6	−178.48 (17)
O1—N3—C1—C2	−165.77 (18)	N5—C4—C5—C2	179.92 (16)
N1—C1—C2—C3	−0.23 (19)	N7—C4—C5—C2	1.5 (3)
N3—C1—C2—C3	177.82 (18)	C1—C2—C5—C4	112.2 (2)
N1—C1—C2—C5	−178.66 (17)	C3—C2—C5—C4	−65.7 (3)
N3—C1—C2—C5	−0.6 (3)	C1—C2—C5—C6	−67.8 (3)
N1—N2—C3—C2	−1.2 (2)	C3—C2—C5—C6	114.2 (2)
N1—N2—C3—N4	−179.43 (16)	N5—N6—C6—C5	0.1 (2)
C1—C2—C3—N2	0.9 (2)	N5—N6—C6—N8	−177.89 (14)
C5—C2—C3—N2	179.30 (18)	C4—C5—C6—N6	−0.04 (19)
C1—C2—C3—N4	178.95 (18)	C2—C5—C6—N6	−179.98 (17)
C5—C2—C3—N4	−2.7 (3)	C4—C5—C6—N8	177.70 (17)
O4—N4—C3—N2	−179.33 (17)	C2—C5—C6—N8	−2.2 (3)
O3—N4—C3—N2	−0.2 (3)	O7—N8—C6—N6	1.3 (2)
O4—N4—C3—C2	2.7 (3)	O8—N8—C6—N6	−179.11 (16)
O3—N4—C3—C2	−178.14 (18)	O7—N8—C6—C5	−176.33 (17)
N6—N5—C4—C5	0.1 (2)	O8—N8—C6—C5	3.3 (3)

Hydrogen-bond geometry (Å, º)

D—H···*A*	*D*—H	H···*A*	*D*···*A*	*D*—H···*A*
N1—H1*N*···O1*W*	0.96 (2)	1.68 (2)	2.634 (2)	177 (3)
N5—H2*N*···O4*W*^{i}	0.97 (2)	1.76 (2)	2.723 (2)	172 (3)
O1*W*—H1···O3*W*	0.87 (2)	2.00 (2)	2.866 (2)	178 (3)
O1*W*—H2···O2*W*	0.87 (2)	1.97 (2)	2.771 (2)	153 (3)
O2*W*—H3···N6^{ii}	0.87 (2)	2.10 (2)	2.942 (2)	164 (3)
O2*W*—H4···O4*W*^{iii}	0.88 (2)	2.07 (2)	2.939 (2)	168 (3)
O3*W*—H5···O3^{iv}	0.86 (2)	2.31 (3)	3.116 (2)	156 (4)
O3*W*—H6···O2*W*^{iii}	0.88 (2)	1.90 (2)	2.766 (2)	170 (3)
O4*W*—H7···O3*W*	0.88 (2)	1.92 (2)	2.779 (2)	166 (3)
O4*W*—H8···O4^{v}	0.88 (2)	2.62 (4)	3.136 (2)	118 (3)
O4*W*—H8···O6^{iv}	0.88 (2)	2.39 (4)	3.051 (2)	132 (4)

Symmetry codes: (i) −*x*, −*y*+1, −*z*+1; (ii) *x*+1/2, −*y*+1/2, −*z*+1; (iii) −*x*+1/2, *y*+1/2, *z*; (iv) *x*, −*y*+3/2, *z*+1/2; (v) *x*, −*y*+1/2, *z*+1/2.

3,3′,5,5′-Tetranitro-4,4′-bipyrazole pentahydrate (2)

Crystal data

$C_6H_2N_8O_8·5H_2O$
M_r = 404.24
Monoclinic, $P2_1/c$
a = 11.2164 (5) Å
b = 20.8114 (6) Å
c = 6.6646 (3) Å
β = 90.435 (4)°
V = 1555.67 (11) Å^3
Z = 4
F(000) = 832
D_x = 1.726 Mg m^{-3}
Cu *Kα* radiation, *λ* = 1.54186 Å
Cell parameters from 14313 reflections
θ = 3.9–80.1°
μ = 1.51 mm^{-1}
T = 183 K
Needle, colorless
0.09 × 0.07 × 0.03 mm

Data collection

STOE STADIVARI diffractometer
Radiation source: GeniX 3D HF Cu
Graded multilayer mirror monochromator
Detector resolution: 5.81 pixels mm^{-1}
rotation method, *ω* scans
Absorption correction: multi-scan (LANA; Koziskova *et al.*, 2016)
T_{min} = 0.787, T_{max} = 0.963
14058 measured reflections
3321 independent reflections
2619 reflections with $I > 2\sigma(I)$
R_{int} = 0.041
θ_{max} = 79.5°, θ_{min} = 3.9°
h = −13→14
k = −9→25
l = −8→8

Refinement

Refinement on F^2
Least-squares matrix: full
$R[F^2 > 2\sigma(F^2)]$ = 0.046
$wR(F^2)$ = 0.128
S = 1.00
3321 reflections
296 parameters
53 restraints
Primary atom site location: structure-invariant direct methods
Secondary atom site location: difference Fourier map
Hydrogen site location: difference Fourier map
H atoms treated by a mixture of independent and constrained refinement
$w = 1/[\sigma^2(F_o^2) + (0.0939P)^2]$ where $P = (F_o^2 + 2F_c^2)/3$
$(\Delta/\sigma)_{max} < 0.001$
$\Delta\rho_{max}$ = 0.42 e Å^{-3}
$\Delta\rho_{min}$ = −0.32 e Å^{-3}

Special details

Geometry. All esds (except the esd in the dihedral angle between two l.s. planes) are estimated using the full covariance matrix. The cell esds are taken into account individually in the estimation of esds in distances, angles and torsion angles; correlations between esds in cell parameters are only used when they are defined by crystal symmetry. An approximate (isotropic) treatment of cell esds is used for estimating esds involving l.s. planes.

Fractional atomic coordinates and isotropic or equivalent isotropic displacement parameters (Å²)

	x	*y*	*z*	U_{iso}*/U_{eq}	Occ. (<1)
O1	0.28035 (12)	−0.04718 (6)	0.3996 (2)	0.0386 (3)	
O2	0.13306 (12)	−0.01590 (6)	0.5861 (2)	0.0392 (3)	
O3	0.37077 (12)	0.25979 (6)	0.3829 (2)	0.0403 (3)	
O4	0.19788 (12)	0.25621 (6)	0.5233 (2)	0.0387 (3)	
O5	−0.13642 (12)	0.21076 (8)	0.3560 (2)	0.0467 (4)	
O6	0.03913 (12)	0.18784 (7)	0.2445 (2)	0.0399 (3)	
O7	0.07786 (14)	0.04766 (7)	1.1095 (2)	0.0438 (4)	
O8	0.23648 (12)	0.07031 (7)	0.9392 (2)	0.0405 (3)	
N1	0.36281 (13)	0.07172 (7)	0.3696 (2)	0.0280 (3)	
N2	0.38173 (13)	0.13466 (7)	0.3548 (2)	0.0283 (3)	
N3	0.22147 (13)	−0.00586 (7)	0.4864 (2)	0.0304 (3)	
N4	0.28528 (13)	0.23088 (7)	0.4509 (2)	0.0296 (3)	
N5	−0.09369 (13)	0.15151 (7)	0.7006 (2)	0.0286 (3)	
N6	−0.05416 (14)	0.11939 (7)	0.8599 (2)	0.0308 (3)	
N7	−0.03690 (13)	0.18720 (7)	0.3731 (2)	0.0307 (3)	
N8	0.12899 (14)	0.07156 (7)	0.9660 (2)	0.0318 (3)	
C1	0.26111 (14)	0.05963 (7)	0.4645 (2)	0.0265 (3)	
C2	0.20628 (15)	0.11677 (7)	0.5198 (2)	0.0259 (3)	
C3	0.28840 (14)	0.16143 (8)	0.4436 (2)	0.0263 (3)	
C4	−0.00963 (14)	0.15605 (8)	0.5601 (3)	0.0267 (3)	
C5	0.09402 (15)	0.12615 (7)	0.6253 (2)	0.0257 (3)	
C6	0.05760 (15)	0.10474 (8)	0.8161 (2)	0.0278 (3)	
O1W	0.54652 (12)	0.00552 (6)	0.2491 (2)	0.0359 (3)	
O3W	0.61658 (12)	0.18711 (6)	0.2917 (2)	0.0379 (3)	
O2W	0.71826 (17)	0.08688 (8)	0.0706 (3)	0.0375 (4)	0.86
O2WA	0.7582 (16)	0.0942 (9)	0.123 (3)	0.059 (4)*	0.14
H3A	0.787930	0.070453	0.214496	0.089*	0.14
H4A	0.812770	0.103103	0.039756	0.089*	0.14
O4W	0.67352 (12)	0.31146 (6)	0.1914 (2)	0.0356 (3)	
O5W	0.49162 (15)	0.38334 (7)	0.3636 (3)	0.0486 (4)	
H3	0.7943 (17)	0.0863 (18)	0.042 (5)	0.058 (10)*	0.86
H4	0.685 (3)	0.088 (2)	−0.041 (4)	0.098 (15)*	0.86
H1	0.603 (2)	0.0235 (11)	0.179 (4)	0.046 (7)*	
H2	0.540 (3)	−0.0326 (10)	0.202 (4)	0.071 (10)*	
H5	0.5436 (16)	0.1760 (12)	0.283 (4)	0.044 (7)*	
H6	0.6573 (19)	0.1615 (11)	0.226 (4)	0.043 (6)*	
H7	0.661 (2)	0.3132 (13)	0.062 (3)	0.053 (8)*	
H8	0.658 (3)	0.2735 (10)	0.228 (4)	0.063 (8)*	
H9	0.5443 (19)	0.3606 (13)	0.306 (4)	0.070 (9)*	

H10	0.434 (2)	0.3591 (14)	0.402 (5)	0.074 (10)*
H1N	0.423 (2)	0.0455 (13)	0.328 (4)	0.048 (7)*
H2N	−0.1678 (19)	0.1639 (11)	0.697 (3)	0.034 (6)*

Atomic displacement parameters (Å²)

	U^{11}	U^{22}	U^{33}	U^{12}	U^{13}	U^{23}
O1	0.0394 (7)	0.0202 (6)	0.0562 (8)	0.0021 (5)	0.0040 (6)	−0.0097 (5)
O2	0.0367 (7)	0.0237 (7)	0.0575 (8)	−0.0042 (5)	0.0111 (6)	0.0005 (5)
O3	0.0370 (7)	0.0225 (7)	0.0616 (9)	−0.0065 (5)	0.0125 (6)	−0.0006 (5)
O4	0.0366 (7)	0.0219 (6)	0.0577 (8)	0.0029 (5)	0.0114 (6)	−0.0038 (5)
O5	0.0273 (7)	0.0508 (9)	0.0620 (9)	0.0069 (6)	0.0011 (6)	0.0231 (7)
O6	0.0334 (7)	0.0463 (8)	0.0401 (7)	0.0019 (6)	0.0057 (5)	0.0096 (6)
O7	0.0470 (8)	0.0434 (8)	0.0409 (7)	−0.0028 (6)	0.0021 (6)	0.0133 (6)
O8	0.0334 (7)	0.0438 (8)	0.0445 (7)	0.0067 (6)	−0.0006 (5)	0.0055 (6)
N1	0.0267 (7)	0.0191 (7)	0.0382 (7)	0.0014 (5)	0.0022 (5)	−0.0027 (5)
N2	0.0290 (7)	0.0189 (7)	0.0369 (7)	−0.0001 (5)	0.0010 (6)	−0.0005 (5)
N3	0.0303 (7)	0.0190 (7)	0.0419 (8)	0.0003 (5)	−0.0008 (6)	−0.0020 (5)
N4	0.0308 (7)	0.0190 (7)	0.0390 (7)	−0.0001 (5)	0.0021 (6)	−0.0012 (5)
N5	0.0252 (7)	0.0198 (7)	0.0408 (7)	0.0010 (5)	0.0049 (5)	0.0007 (5)
N6	0.0321 (8)	0.0232 (7)	0.0372 (7)	0.0000 (5)	0.0035 (6)	0.0012 (5)
N7	0.0249 (7)	0.0246 (7)	0.0425 (8)	−0.0025 (5)	0.0000 (6)	0.0055 (6)
N8	0.0365 (8)	0.0233 (7)	0.0358 (7)	0.0018 (6)	−0.0004 (6)	0.0002 (5)
C1	0.0270 (8)	0.0179 (8)	0.0346 (8)	−0.0003 (6)	0.0006 (6)	−0.0011 (6)
C2	0.0269 (8)	0.0187 (7)	0.0319 (7)	0.0011 (6)	−0.0009 (6)	−0.0010 (5)
C3	0.0269 (8)	0.0176 (8)	0.0343 (8)	0.0000 (6)	0.0011 (6)	−0.0016 (6)
C4	0.0257 (8)	0.0181 (8)	0.0364 (8)	−0.0008 (5)	0.0020 (6)	0.0009 (6)
C5	0.0258 (8)	0.0166 (7)	0.0347 (8)	−0.0012 (5)	0.0020 (6)	−0.0013 (5)
C6	0.0317 (8)	0.0190 (7)	0.0327 (8)	−0.0001 (6)	0.0012 (6)	0.0007 (6)
O1W	0.0340 (7)	0.0238 (7)	0.0500 (7)	0.0026 (5)	0.0070 (6)	−0.0027 (5)
O3W	0.0277 (7)	0.0249 (7)	0.0611 (9)	−0.0023 (5)	0.0034 (6)	−0.0020 (5)
O2W	0.0347 (9)	0.0337 (9)	0.0442 (10)	−0.0025 (7)	0.0040 (8)	0.0027 (7)
O4W	0.0305 (7)	0.0222 (7)	0.0542 (8)	−0.0005 (5)	0.0048 (5)	0.0046 (5)
O5W	0.0492 (9)	0.0228 (7)	0.0741 (11)	−0.0007 (6)	0.0115 (8)	0.0004 (6)

Geometric parameters (Å, º)

O1—N3	1.2313 (19)	N8—C6	1.451 (2)
O2—N3	1.216 (2)	C1—C2	1.390 (2)
O3—N4	1.2221 (19)	C2—C3	1.406 (2)
O4—N4	1.2161 (19)	C2—C5	1.460 (2)
O5—N7	1.2236 (19)	C4—C5	1.386 (2)
O6—N7	1.2134 (19)	C5—C6	1.411 (2)
O7—N8	1.224 (2)	O1W—H1	0.872 (18)
O8—N8	1.220 (2)	O1W—H2	0.855 (19)
N1—N2	1.331 (2)	O3W—H5	0.852 (17)
N1—C1	1.332 (2)	O3W—H6	0.828 (17)
N1—H1N	0.92 (3)	O2W—H3	0.875 (19)

N2—C3	1.329 (2)	O2W—H4	0.83 (2)
N3—C1	1.441 (2)	O2WA—H3A	0.8500
N4—C3	1.447 (2)	O2WA—H4A	0.8500
N5—N6	1.328 (2)	O4W—H7	0.875 (17)
N5—C4	1.337 (2)	O4W—H8	0.845 (19)
N5—H2N	0.87 (2)	O5W—H9	0.851 (19)
N6—C6	1.325 (2)	O5W—H10	0.861 (19)
N7—C4	1.436 (2)		

N2—N1—C1	111.01 (13)	C5—C4—N7	130.37 (15)
N2—N1—H1N	116.4 (17)	C4—C5—C6	100.17 (14)
C1—N1—H1N	132.1 (17)	C4—C5—C2	129.33 (15)
C3—N2—N1	104.66 (14)	C6—C5—C2	130.42 (15)
O2—N3—O1	125.39 (15)	N6—C6—C5	114.03 (15)
O2—N3—C1	118.13 (14)	N6—C6—N8	118.41 (15)
O1—N3—C1	116.48 (15)	C5—C6—N8	127.53 (15)
O4—N4—O3	124.81 (15)	H1—O1W—H2	105 (2)
O4—N4—C3	117.78 (14)	H5—O3W—H6	109 (2)
O3—N4—C3	117.40 (14)	O2WA—O2W—H3A	33.1
N6—N5—C4	111.26 (14)	O2WA—O2W—H4A	47.1
N6—N5—H2N	119.0 (15)	H3A—O2W—H4A	69.4
C4—N5—H2N	129.6 (14)	O2WA—O2W—H3	53 (2)
C6—N6—N5	104.48 (14)	H3A—O2W—H3	64.5
O6—N7—O5	125.14 (16)	H4A—O2W—H3	18.2
O6—N7—C4	118.13 (14)	O2WA—O2W—H4	149 (3)
O5—N7—C4	116.72 (15)	H3A—O2W—H4	161.5
O8—N8—O7	125.10 (16)	H4A—O2W—H4	103.8
O8—N8—C6	116.73 (15)	H3—O2W—H4	104 (3)
O7—N8—C6	118.17 (15)	O2W—O2WA—H3A	124.8
N1—C1—C2	110.28 (14)	O2W—O2WA—H4A	102.5
N1—C1—N3	119.50 (14)	H3A—O2WA—H4A	108.4
C2—C1—N3	130.14 (15)	O2W—O2WA—H3	86 (3)
C1—C2—C3	100.21 (14)	H3A—O2WA—H3	101.1
C1—C2—C5	128.84 (15)	H4A—O2WA—H3	28.3
C3—C2—C5	130.94 (14)	O2W—O2WA—H4	18 (2)
N2—C3—C2	113.84 (14)	H3A—O2WA—H4	138.6
N2—C3—N4	116.95 (14)	H4A—O2WA—H4	85.7
C2—C3—N4	129.21 (15)	H3—O2WA—H4	73 (3)
N5—C4—C5	110.06 (15)	H7—O4W—H8	107 (2)
N5—C4—N7	119.54 (15)	H9—O5W—H10	110 (2)

C1—N1—N2—C3	−0.03 (18)	N6—N5—C4—N7	177.78 (14)
C4—N5—N6—C6	0.81 (18)	O6—N7—C4—N5	−176.42 (15)
N2—N1—C1—C2	−0.29 (19)	O5—N7—C4—N5	3.1 (2)
N2—N1—C1—N3	176.78 (14)	O6—N7—C4—C5	1.5 (3)
O2—N3—C1—N1	174.75 (15)	O5—N7—C4—C5	−178.95 (17)
O1—N3—C1—N1	−6.0 (2)	N5—C4—C5—C6	0.08 (18)
O2—N3—C1—C2	−8.8 (3)	N7—C4—C5—C6	−178.03 (17)

O1—N3—C1—C2	170.46 (17)	N5—C4—C5—C2	177.08 (15)
N1—C1—C2—C3	0.46 (17)	N7—C4—C5—C2	−1.0 (3)
N3—C1—C2—C3	−176.22 (17)	C1—C2—C5—C4	−117.2 (2)
N1—C1—C2—C5	179.77 (16)	C3—C2—C5—C4	61.9 (3)
N3—C1—C2—C5	3.1 (3)	C1—C2—C5—C6	58.9 (3)
N1—N2—C3—C2	0.35 (19)	C3—C2—C5—C6	−122.0 (2)
N1—N2—C3—N4	179.72 (14)	N5—N6—C6—C5	−0.78 (19)
C1—C2—C3—N2	−0.50 (18)	N5—N6—C6—N8	177.12 (14)
C5—C2—C3—N2	−179.79 (16)	C4—C5—C6—N6	0.44 (19)
C1—C2—C3—N4	−179.78 (16)	C2—C5—C6—N6	−176.50 (15)
C5—C2—C3—N4	0.9 (3)	C4—C5—C6—N8	−177.23 (16)
O4—N4—C3—N2	176.67 (15)	C2—C5—C6—N8	5.8 (3)
O3—N4—C3—N2	−3.1 (2)	O8—N8—C6—N6	−165.51 (15)
O4—N4—C3—C2	−4.1 (3)	O7—N8—C6—N6	13.8 (2)
O3—N4—C3—C2	176.20 (17)	O8—N8—C6—C5	12.1 (3)
N6—N5—C4—C5	−0.57 (19)	O7—N8—C6—C5	−168.60 (16)

Hydrogen-bond geometry (Å, º)

D—H···*A*	*D*—H	H···*A*	*D*···*A*	*D*—H···*A*
N1—H1*N*···O1*W*	0.92 (3)	1.70 (3)	2.610 (2)	173 (3)
N5—H2*N*···O4*W*^{i}	0.87 (2)	1.85 (2)	2.723 (2)	179 (2)
O1*W*—H1···O2*W*	0.87 (2)	1.99 (2)	2.833 (2)	163 (2)
O1*W*—H2···O5*W*^{ii}	0.86 (2)	1.84 (2)	2.685 (2)	170 (3)
O2*W*—H3···N6^{iii}	0.88 (2)	2.21 (3)	3.000 (2)	151 (3)
O2*W*—H4···O5*W*^{iv}	0.83 (2)	2.33 (3)	2.949 (3)	131 (3)
O2*W*—H4···O1^{v}	0.83 (2)	2.57 (3)	3.241 (3)	139 (3)
O3*W*—H5···N2	0.85 (2)	2.07 (2)	2.885 (2)	160 (2)
O3*W*—H6···O2*W*	0.83 (2)	1.99 (2)	2.802 (2)	166 (2)
O4*W*—H7···O3*W*^{iv}	0.88 (2)	1.87 (2)	2.735 (2)	173 (2)
O4*W*—H8···O3*W*	0.85 (2)	1.91 (2)	2.749 (2)	176 (3)
O5*W*—H9···O4*W*	0.85 (2)	1.94 (2)	2.784 (2)	175 (3)
O5*W*—H10···O3	0.86 (2)	2.19 (3)	2.910 (2)	141 (3)
O5*W*—H10···O8^{iv}	0.86 (2)	2.67 (3)	3.065 (2)	109 (2)

Symmetry codes: (i) *x*−1, −*y*+1/2, *z*+1/2; (ii) −*x*+1, *y*−1/2, −*z*+1/2; (iii) *x*+1, *y*, *z*−1; (iv) *x*, −*y*+1/2, *z*−1/2; (v) −*x*+1, −*y*, −*z*.